Journal of Structural Geology 30 (2008) 1150–1166

Contents lists available at ScienceDirect

Journal of Structural Geology

journal homepage: www.elsevier.com/locate/jsg

Mylonitic deformation of gabbro in the lower crust: A case study from the Pankenushi gabbro in the Hidaka metamorphic belt of central Hokkaido, Japan

Kyuichi Kanagawa*, Hirobumi Shimano [1], Yoshikuni Hiroi

Department of Earth Sciences, Chiba University, Yayoi-cho 1-33, Inage-ku, Chiba 263-8522, Japan

ARTICLE INFO

Article history:
Received 21 April 2007
Received in revised form 17 May 2008
Accepted 19 May 2008
Available online 29 May 2008

Keywords:
Mylonite
Gabbro
Dynamic recrystallization
Reaction
Crystal plasticity
Grain boundary sliding

ABSTRACT

The mylonitization of the Pankenushi gabbro in the Hidaka metamorphic belt of central Hokkaido, Japan, occurred along its western margin at ≈600 MPa and 660–700 °C through dynamic recrystallization of plagioclase and a retrograde reaction from granulite facies to amphibolite facies (orthopyroxene + clinopyroxene + plagioclase + H_2O = hornblende + quartz). The reaction produced a fine-grained (≤100 μm) polymineralic aggregate composed of orthopyroxene, clinopyroxene, quartz, hornblende, biotite and ilmenite, into which strain is localized. The dynamic recrystallization of plagioclase occurred by grain boundary migration, and produced a monomineralic aggregate of grains whose crystallographic orientations are mostly unrelated to those of porphyroclasts. The monomineralic plagioclase aggregates and the fine-grained polymineralic aggregates are interlayered and define the mylonitic foliation, while the latter is also mixed into the former by grain boundary sliding to form a rather homogeneous polymineralic matrix in ultramylonites. However in both mylonite and ultramylonite, plagioclase aggregates form a stress-supporting framework, and therefore controlled the rock rheology. Crystal plastic deformation of pyroxenes and plagioclase with dominant (100)[001] and (001)1/2<1$\bar{1}$0> slip systems, respectively, produced distinct shape- and crystallographic-preferred orientations of pyroxene porphyroclasts and dynamically recrystallized plagioclase grains in both mylonite and ultramylonite. Euhedral to subhedral growth of hornblende in pyroxene porphyroclast tails during the reaction and its subsequent rigid rotation in the fine-grained polymineralic aggregate or matrix produced clear shape- and crystallographic-preferred orientations of hornblende grains in both mylonite and ultramylonite. In contrast, the dominant grain boundary sliding of pyroxene and quartz grains in the fine-grained polymineralic aggregate of the mylonite resulted in their very weak shape- and crystallographic-preferred orientations. In the fine-grained polymineralic matrix of the ultramylonite, however, pyroxene and quartz grains became scattered and isolated in the plagioclase aggregate so that they were crystal-plastically deformed leading to stronger shape- and crystallographic-preferred orientations than those seen in the mylonite.

1. Introduction

Since gabbro is thought to be a common rock type found in the continental lower crust, its mylonitic deformation under elevated pressure–temperature conditions is important not only structurally in terms of deformation and strain localization processes in the lower crust, but also rheologically in terms of the strength and mechanical behavior of the lower crust (e.g. Rutter and Brodie, 1992). Previous studies of gabbroic mylonites formed at lower crustal conditions revealed crystal plastic deformation and dynamic recrystallization of plagioclase (e.g. Jensen and Starkey, 1985; Olsen and Kohlstedt, 1985; Olesen, 1987; Ji and Mainprice, 1990; Dornbusch et al., 1994; Kruse and Stünitz, 1999; Kruse et al., 2001; Baratoux et al., 2005), crystal plastic deformation of pyroxenes (e.g. Dornbusch et al., 1994; Kenkmann, 2000), and nucleation and growth of amphibole (e.g. Kruse and Stünitz, 1999; Kenkmann and Dresen, 2002; Baratoux et al., 2005). Other studies emphasized the role of syntectonic breakdown reactions of pyroxenes or garnet (e.g. Beach, 1980; Brodie, 1995; Stünitz, 1998; Kruse and Stünitz, 1999; Kenkmann, 2000). However, the dynamic recrystallization, dominant slip systems and crystallographic-preferred orientations of plagioclase are still not well understood even though plagioclase is the most abundant mineral found in the crust (e.g. Tullis, 2002). In addition, the deformation behavior of other constituent minerals such as pyroxenes and amphibole in gabbroic mylonites is still poorly understood (e.g. Dornbusch et al., 1994; Kenkmann and Dresen, 2002).

* Corresponding author. Tel.: +81 43 290 2857; fax: +81 43 290 2859.
E-mail address: kyu_kanagawa@faculty.chiba-u.jp (K. Kanagawa).
[1] Present address: Exploration and Production Division, Eni S.p.A., Via Emilia 1, San Donato Milanese, MI 20097, Italy.

0191-8141/$ – see front matter © 2008 Elsevier Ltd. All rights reserved.
doi:10.1016/j.jsg.2008.05.007

This paper describes the grain-scale processes during mylonitization of the Pankenushi gabbro in the Hidaka metamorphic belt of central Hokkaido, Japan, which occurred at ≈600 MPa and 660–700 °C. Microstructural observations and a large amount of shape- and crystallographic-orientation data for the constituent minerals in two representative samples provide important new information concerning the deformation behavior of plagioclase and other constituent minerals in gabbro under lower crustal conditions.

2. Geological setting

The Hidaka metamorphic belt of south–central Hokkaido, Japan (Fig. 1a) lies within a zone of collision between the Kuril arc and the Northeast Japan arc since the early Tertiary (e.g. Komatsu et al., 1983; Kimura, 1986). The Hidaka metamorphic Main Zone (e.g. Fig. 1b) represents a partial section through the ancient Kuril arc crust, the upper 23 km of which is exposed at the surface along the Hidaka Main Thrust (HMT; Fig. 1b) (Komatsu et al., 1983). The Main Zone consists of felsic and mafic metamorphic rocks, and plutonic rocks such as gabbro, diorite and tonalite (Komatsu et al., 1983; Osanai et al., 1991). The metamorphic grade gradually decreases eastwards from granulite through amphibolite to greenschist facies (Osanai et al., 1991). The footwall of the Hidaka Main Thrust is either the Hidaka metamorphic Western Zone or the Idon'nappu belt (e.g. Fig. 1b). The Western Zone is narrow (≤4 km), and consists mainly of greenschist, amphibolite and metagabbro, which collectively are interpreted to form a meta-ophiolitic assemblage (Miyashita, 1983). The Western Zone lies in thrust contact with the Idon'nappu belt along the Western Boundary Thrust (WBT; Fig. 1b). The Idon'nappu belt is composed of an accretionary mélange of Cretaceous to Paleocene age (Kiyokawa, 1992; Ueda et al., 1993).

The Pankenushi gabbro in the northern part of the Hidaka metamorphic Main Zone (Fig. 1a) is mylonitized along its western margin by dextral shearing (Toyoshima et al., 1994; Toyoshima, 1998). It is considered to have been intruded concurrently with anatexis of the Main Zone rocks (Maeda and Kagami, 1996) which has been dated at approximately 55 Ma (Owada et al., 1991) and corresponds to a metamorphic peak in the Main Zone (Komatsu et al., 1994). The exhumation of the Main Zone rocks along the Hidaka Main Thrust is estimated to have occurred approximately at 17 Ma (Arita et al., 1993). Hence the mylonitization of the Pankenushi gabbro occurred sometime between 55 Ma and 17 Ma.

In the Pankenushi river area, the western margin of the Pankenushi gabbro together with felsic granulite in contact with the gabbro are mylonitized in a 200–300 m wide zone (Fig. 1b), where a N- to NNW-trending, subvertical mylonitic foliation and a subhorizontal mylonitic lineation are developed (Fig. 1c). We collected two representative mylonite samples along the Pankenushi trail for detail analyses in this study (Fig. 1b): a gabbro mylonite sample (GbM) and a gabbro ultramylonite sample (GbUM). In addition, we collected a sample of garnet–biotite gneiss (GBGn; Fig. 1b) to constrain pressure–temperature conditions from immediately adjacent metamorphic rocks.

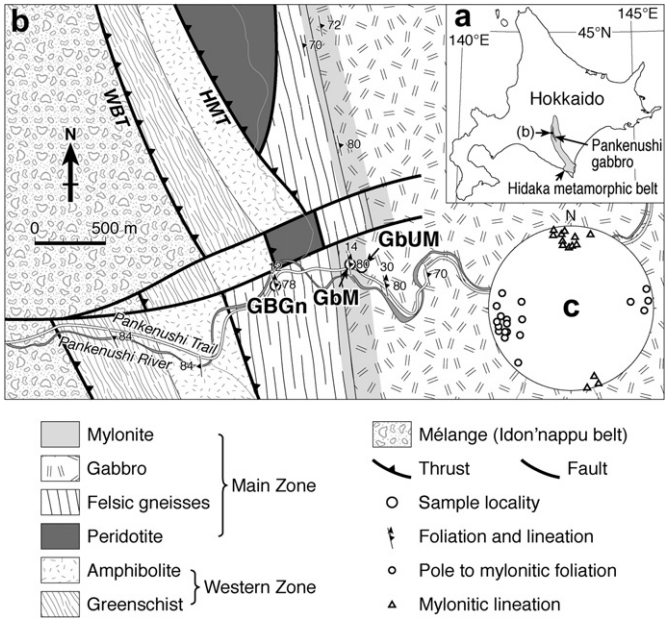

Fig. 1. (a) Index map showing locations of the Hidaka metamorphic belt, the Pankenushi gabbro and the study area (b). (b) Geologic map of the study area, where three sample localities (GbM, GbUM and GBGn) are shown. *HMT*, Hidaka Main Thrust; *WBT*, Western Boundary Thrust. (c) Equal-area, lower-hemisphere projections of mylonitic foliation (19 data) and lineation (14 data) measured at several localities.

3. Microstructures

Microstructures in the gabbro mylonite samples were observed by means of optical and back-scattered electron (BSE) microscopy, viewing thin sections cut perpendicular to the mylonitic foliation and parallel to the mylonitic lineation.

3.1. Gabbro mylonite sample (GbM)

This sample contains porphyroclasts of orthopyroxene, clinopyroxene and plagioclase set in a matrix of either fine-grained (≤150 μm) monomineralic plagioclase grains or a fine-grained (≤100 μm) polymineralic aggregate (Fig. 2a). These two matrix types alternate in layers to define the mylonitic foliation, while elongate pyroxene porphyroclasts primarily delineate the mylonitic lineation (Fig. 2a; cf. Toyoshima, 1998).

Pyroxene porphyroclasts commonly contain lamellae or inclusions of ilmenite and exsolution lamellae (Fig. 2a,d). They exhibit undulose extinction and bending, but subgrain boundaries and bulging grain boundaries are not observed. Asymmetric tails of orthopyroxene, clinopyroxene, quartz, hornblende, biotite and ilmenite grains indicate a dextral sense of shear (Fig. 2a,c,d). Lobate quartz grains are commonly distributed around pyroxene porphyroclasts along their foliation-subparallel boundaries, while euhedral to subhedral hornblende and biotite grains are common in porphyroclast tails (Fig. 2c–e). Pyroxene porphyroclast rims are locally isolated or almost isolated by the presence of quartz, hornblende and biotite grains (Fig. 2c,d).

Plagioclase porphyroclasts exhibit undulose extinction and deformation twinning, and are surrounded by finer, monomineralic-aggregate plagioclase grains (Fig. 2b). The latter are polygonal in shape, and commonly have subgrain boundaries and bulging grain boundaries (Fig. 2f), while they rarely exhibit deformation twins.

The fine-grained polymineralic aggregate comprises orthopyroxene, clinopyroxene, quartz, hornblende, biotite and ilmenite (Fig. 2a,g). They are derived from pyroxene porphyroclast tails, and those derived from orthopyroxene porphyroclast tails are rich in orthopyroxene (e.g. Fig. 2g), while those derived from clinopyroxene porphyroclast tails are rich in clinopyroxene.

3.2. Gabbro ultramylonite sample (GbUM)

This sample contains a few pyroxene porphyroclasts set in a fine-grained polymineralic matrix of plagioclase, orthopyroxene, clinopyroxene, quartz, hornblende, biotite and ilmenite (Fig. 3a,b). Orthopyroxene porphyroclasts are markedly elongate, whereas clinopyroxene porphyroclasts are less elongate (e.g. Fig. 3a). Plagioclase porphyroclasts are absent. In the fine-grained

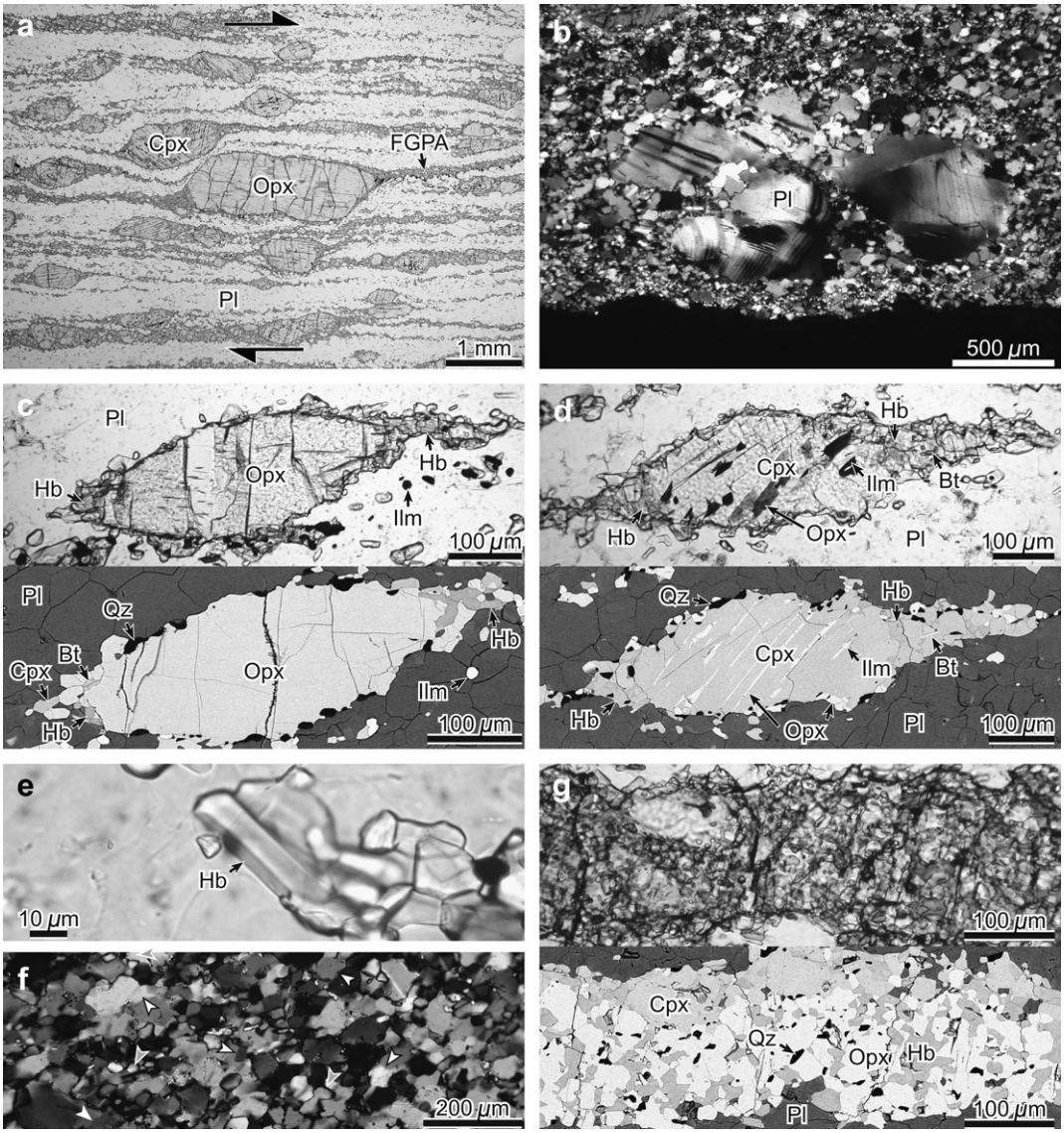

Fig. 2. Microstructures of the sample GbM. Foliation trace and lineation are horizontal in all the micrographs shown. For mineral abbreviations see Table 1. (a) Optical micrograph (plane-polarized light; PPL) showing a porphyroclast-in-matrix microstructure. Asymmetric tails of pyroxene porphyroclasts indicate a dextral sense of shear as shown by a pair of arrows. (b) Optical micrograph (crossed-polarized light; CPL) of a plagioclase porphyroclast (center) showing undulose extinction and deformation twinning, and being surrounded by finer plagioclase grains. (c) Optical (PPL; upper) and BSE (lower) micrographs of an orthopyroxene porphyroclast surrounded by lobate quartz grains along the foliation-subparallel boundary, while by elongate hornblende and biotite grains in its tails. (d) Optical (PPL; upper) and BSE (lower) micrographs of a clinopyroxene porphyroclast with the same occurrence of quartz, hornblende and biotite as around the orthopyroxene porphyroclast in (c). (e) Optical micrograph (PPL) of a euhedral hornblende grain. (f) Optical micrograph (CPL) of a monomineralic plagioclase aggregate with subgrain boundaries (white arrowheads) and bulging grain boundaries (gray arrowheads). (g) Optical (PPL; upper) and BSE (lower) micrographs of a fine-grained polymineralic aggregate derived from an orthopyroxene porphyroclast.

polymineralic matrix, orthopyroxene, clinopyroxene, quartz, hornblende, biotite and ilmenite grains are scattered in an aggregate dominated by plagioclase (Fig. 3a,b). Asymmetric tails around pyroxene porphyroclasts indicate a dextral sense of shear (Fig. 3a,c,d), and lobate quartz grains and euhedral to subhedral hornblende grains are distributed around pyroxene porphyroclasts along their foliation-subparallel boundaries and in their tails, respectively (Fig. 3c,d).

4. Modal compositions and grain sizes

4.1. Data acquisition

Modal composition and grain size data (Table 1) were obtained from thin sections without corrections for sectioning effects being made. Modal contents of porphyroclasts were obtained by digitally tracing them from optical micrographs and calculating their area fractions. The modal content of the monomineralic plagioclase aggregate in the sample GbM was determined by point counting with a traverse spacing of 250 μm. From these results, the modal content of the fine-grained polymineralic aggregate or matrix was calculated. The modal content of each mineral species in the aggregate or matrix was derived using the area fraction of the grains digitally traced from BSE micrographs referring to orientation contrast images (cf. Prior et al., 1996) in order to distinguish grain boundaries.

The diameter of a circle having an area equal to that of a grain was used to derive grain size, which was obtained by image analysis of the grain digitally traced from either optical or BSE micrograph using Wayne Rasband's software (NIH Image 1.63).

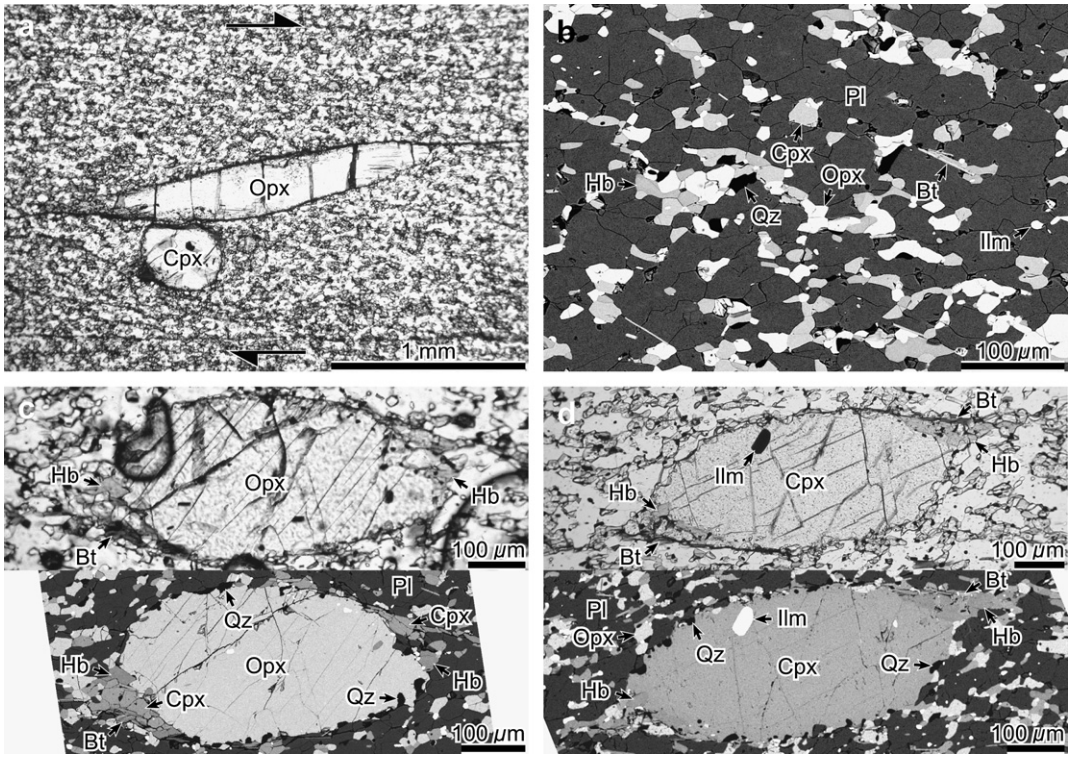

Fig. 3. Microstructures of the sample GbUM. Foliation trace and lineation are horizontal in all the micrographs shown. For mineral abbreviations see Table 1. (a) Optical micrograph (PPL) showing an elongate orthopyroxene porphyroclast and a rounded clinopyroxene porphyroclast in a rather homogeneous matrix. Asymmetric tails of pyroxene porphyroclasts indicate a dextral sense of shear as shown by a pair of arrows. (b) BSE micrograph of a fine-grained polymineralic matrix in which orthopyroxene, clinopyroxene, quartz, hornblende, biotite and ilmenite grains are scattered in a plagioclase aggregate. (c) Optical (PPL; upper) and BSE (lower) micrographs of an orthopyroxene porphyroclast surrounded by lobate quartz grains along the foliation-subparallel boundary, while by elongate hornblende and biotite grains in its tails. (d) Optical (PPL; upper) and BSE (lower) micrographs of a clinopyroxene porphyroclast with the same occurrence of quartz, hornblende and biotite as around the orthopyroxene porphyroclast in (c).

4.2. Modal compositions

The samples of GbM and GbUM have very similar modal mineralogies: ≈65% plagioclase, 18–20% orthopyroxene, ≈10% clinopyroxene, 2–3% hornblende, ≈1% quartz, 0.3–1% biotite, and 0.5–2% ilmenite (Table 1). GbUM is richer in biotite and ilmenite, and slightly poorer in orthopyroxene. The modal content of porphyroclasts decreases with increasing mylonitization from ≈12% in GbM to ≈5% in GbUM (Table 1). GbM contains 0.6% porphyroclast plagioclase, whereas it is absent in GbUM. In the fine-grained

Table 1
Modal compositions and grain sizes of the two gabbro mylonite samples

Mineral species	Microstructural domain	GbM						GbUM					
		Mode (%)	Grain size (μm)					Mode (%)	Grain size (μm)				
			N	Max	Min	Ave	SD		*N*	Max	Min	Ave	SD
Opx	Pc	10.49	835	972.0	97.7	328.7	150.2	4.06	643	1198.7	74.8	254.5	162.9
	FGPA/Mx	9.80	1667	101.7	1.1	16.0	11.4	13.58	1510	42.5	2.8	13.8	6.4
Cpx	Pc	1.29	158	755.3	106.2	266.6	116.9	1.05	108	1130.6	82.8	301.9	222.2
	FGPA/Mx	9.12	1200	97.1	3.1	18.3	12.6	8.89	1084	35.7	3.3	13.3	5.9
Pl	Pc	0.59	28	1173.3	203.5	430.1	186.7	0.00	–	–	–	–	–
	MA	64.34	1955	153.2	3.9	32.5	18.4	0.00	–	–	–	–	–
	FGPA/Mx	0.00	–	–	–	–	–	65.45	2435	74.3	3.5	23.4	11.9
Qz	FGPA/Mx	1.26	1005	28.8	1.2	7.9	4.3	1.10	564	16.8	1.4	6.3	3.1
Hb	FGPA/Mx	2.29	1087	61.3	2.6	10.3	5.5	2.76	570	39.1	2.9	10.2	4.5
Bt	FGPA/Mx	0.33	320	19.9	2.8	7.6	3.1	1.09	344	21.4	2.4	8.4	3.1
Ilm	FGPA/Mx	0.49	467	38.6	1.5	7.0	4.4	2.02	1622	15.4	1.2	5.1	2.4
	Pc	12.37	1021	1173.3	97.7	321.9	149.3	5.10	751	1198.7	74.8	261.3	173.3
	Mx	87.63	7701	153.2	1.1	17.8	15.3	94.90	8129	74.3	1.2	13.9	10.3
	FGPA/Mx w/o Pl	23.29	5746	101.7	1.1	12.8	10.0	29.45	5694	42.5	1.2	9.8	6.1

Opx, orthopyroxene; Cpx, clinopyroxene; Pl, plagioclase; Qz, quartz; Hb, hornblende; Bt, biotite; Ilm, ilmenite; Pc, porphyroclast; MA, monomineralic aggregate; FGPA, fine-grained polymineralic aggregate; Mx, matrix; FGPA/Mx, fine-grained polymineralic aggregate for the sample GbM and matrix for the sample GbUM; FGPA/Mx w/o Pl, fine-grained polymineralic aggregate for the sample GbM and matrix other than plagioclase for the sample GbUM; *N*, number of grains measured; Max, maximum grain size; Min, minimum grain size; Ave, average grain size; SD, standard deviation.

polymineralic aggregate or matrix, the modal content of orthopyroxene increases with mylonitization, whereas those of clinopyroxene, hornblende and quartz remain roughly constant (Table 1).

4.3. Grain sizes

Porphyroclasts in the samples of GbM and GbUM range in size from 75 μm to 1200 μm with no clear difference between the two (Table 1). Monomineralic-aggregate plagioclase grains in GbM have an average size of ≈33 μm, while matrix plagioclase grains in GbUM have an average size of ≈23 μm (Table 1). Grains of constituent minerals other than plagioclase in the fine-grained polymineralic aggregate or matrix are smaller than 102 μm, and their average sizes (10–13 μm) do not show noticeable changes with increasing mylonitization, although the maximum sizes decrease (Table 1).

5. Shape orientation data

5.1. Data acquisition and processing

The aspect ratio (R) and long-axis orientation (φ) data for constituent minerals other than biotite and ilmenite were obtained by

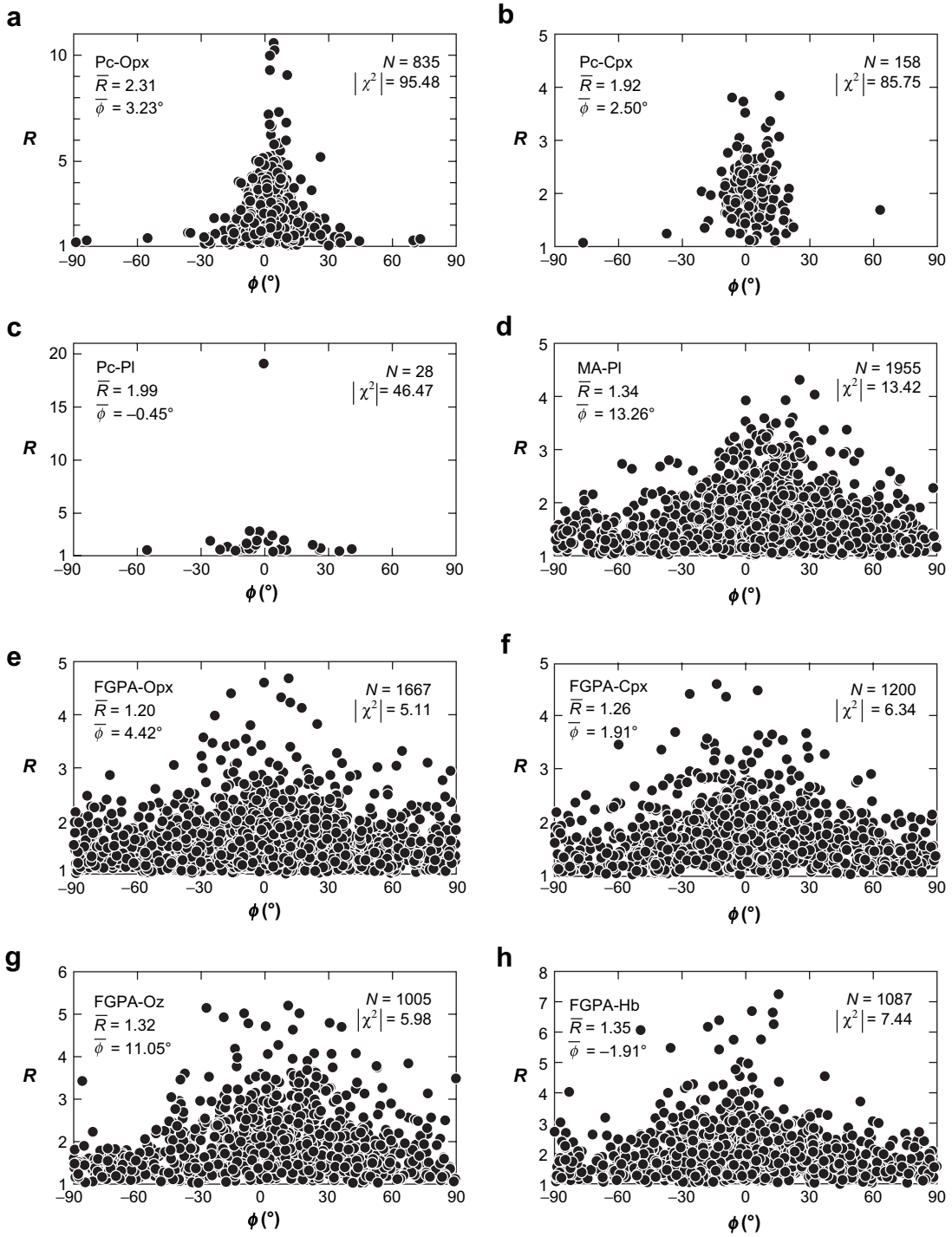

Fig. 4. R/φ diagrams of constituent mineral grains in the sample GbM. N, number of grains measured; $|\chi^2|$, normalized χ^2 value; $\overline{R}$ and $\overline{\phi}$, R and φ of a Wheeler's (1984) average ellipse. See Table 1 for the abbreviations of minerals and microstructural domains.

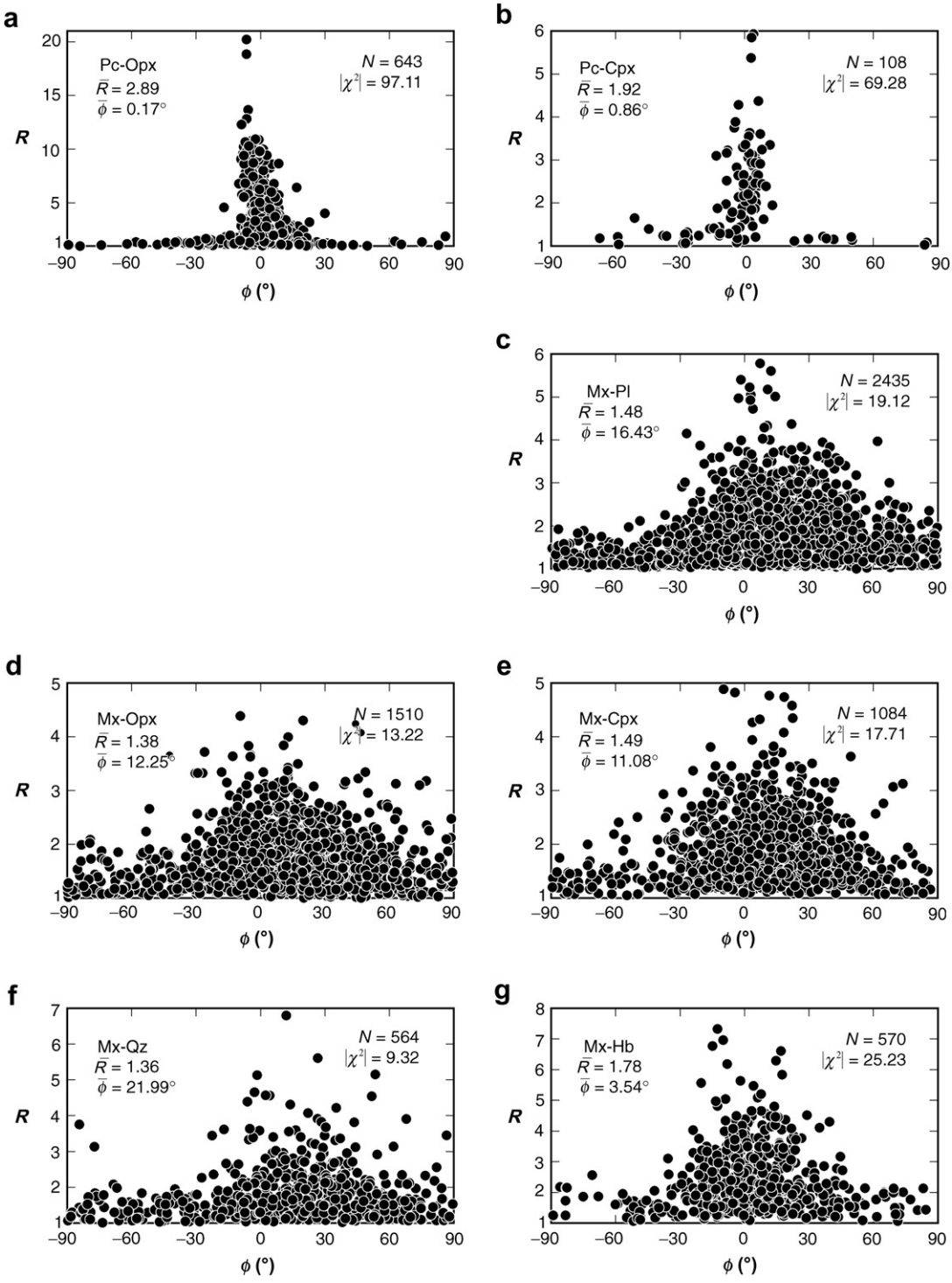

Fig. 5. R/φ diagrams of constituent mineral grains in the sample GbUM. *N*, number of grains measured; $|\chi^2|$, normalized χ^2 value; $\bar{R}$ and $\bar{\phi}$, *R* and φ of a Wheeler's (1984) average ellipse. See Table 1 for the abbreviations of minerals and microstructural domains.

image analyses of digitally traced grains using NIH Image 1.63. φ was measured anticlockwise from the foliation trace in thin sections. For each mineral species in different microstructural domains, aspect ratios were plotted against long-axis orientations on R/φ diagrams (Figs. 4 and 5).

We calculated an average ellipse from individual R/φ data by averaging ellipse shape tensors (Wheeler, 1984), and its *R* and φ ($\bar{R}$ and $\bar{\phi}$ in Figs. 4 and 5) from eigenvalues and eigenvectors of the averaged ellipse shape tensor. The χ^2 value for a φ distribution with 18 cells at 10° intervals normalized by the number of grains in a cell expected for a uniform φ distribution, $|\chi^2|$, was used as a measure of the strength of a shape-preferred orientation (SPO).

5.2. Gabbro mylonite sample (GbM)

Porphyroclast pyroxenes exhibit strong ($|\chi^2| \geq 85$) SPOs subparallel to the foliation trace (Fig. 4a,b). Orthopyroxene porphyroclasts are elongate with aspect ratios of up to 10.6, while clinopyroxene

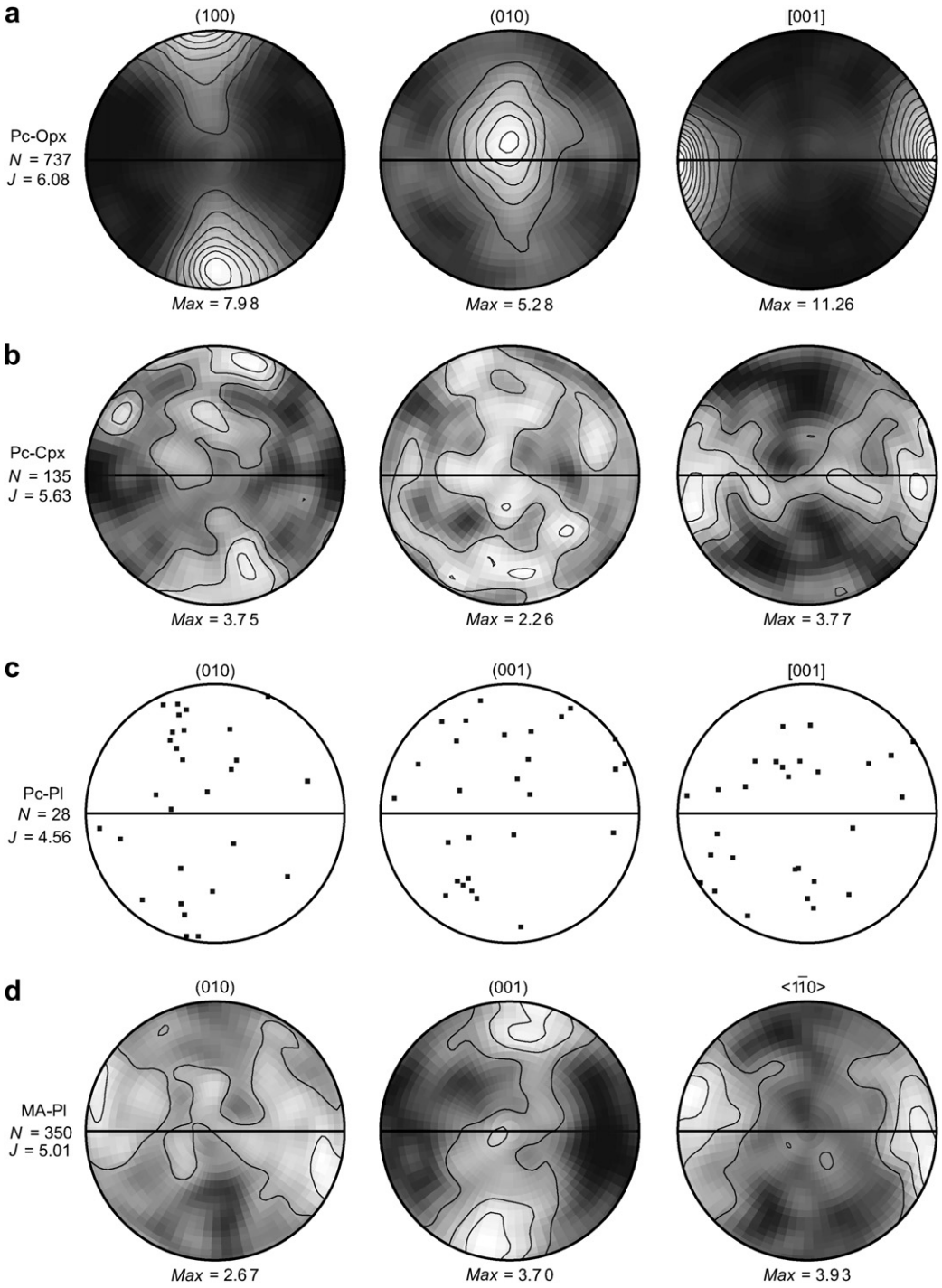

Fig. 6. Crystallographic orientations of constituent mineral grains in the sample GbM. Equal-area, lower hemisphere projections using David Mainprice's Pf2k. Contoured at multiples of uniform distribution and shaded brighter for higher densities. In each stereogram, foliation is indicated by a horizontal line with lineation direction at its ends. *N*, number of grains measured; *J*, *J*-index value; *Max*, maximum density normalized by uniform distribution. See Table 1 for the abbreviations of minerals and microstructural domains.

porphyroclasts are less elongate with aspect ratios of up to 3.9. Porphyroclast plagioclase also shows an SPO subparallel to the foliation trace with a large $|\chi^2|$ value of ≈46 (Fig. 4c). Except for an extremely elongate porphyroclast with an aspect ratio of 19.2, plagioclase porphyroclasts have aspect ratios smaller than 3.4 (Fig. 4c).

Monomineralic-aggregate plagioclase exhibits a moderate ($|\chi^2| \approx 13$) SPO anticlockwise oblique to the foliation trace (Fig. 4d). Provided that the plagioclase grains are dynamically recrystallized, this oblique foliation suggests a dextral sense of shear as also indicated by asymmetric tails around pyroxene porphyroclasts.

In the fine-grained polymineralic aggregate, pyroxenes do not show well defined SPOs having very small $|\chi^2|$ values of around 6 (Fig. 4e,f), in marked contrast to porphyroclast pyroxenes. Quartz also exhibits a very weak ($|\chi^2| \approx 6$) SPO (Fig. 4g). Hornblende shows a weak ($|\chi^2| \approx 7$) SPO subparallel to the foliation trace (Fig. 4h).

5.3. Gabbro ultramylonite sample (GbUM)

As in the sample GbM, porphyroclast pyroxenes exhibit strong ($|\chi^2| \geq 69$) SPOs subparallel to the foliation trace (Fig. 5a,b).

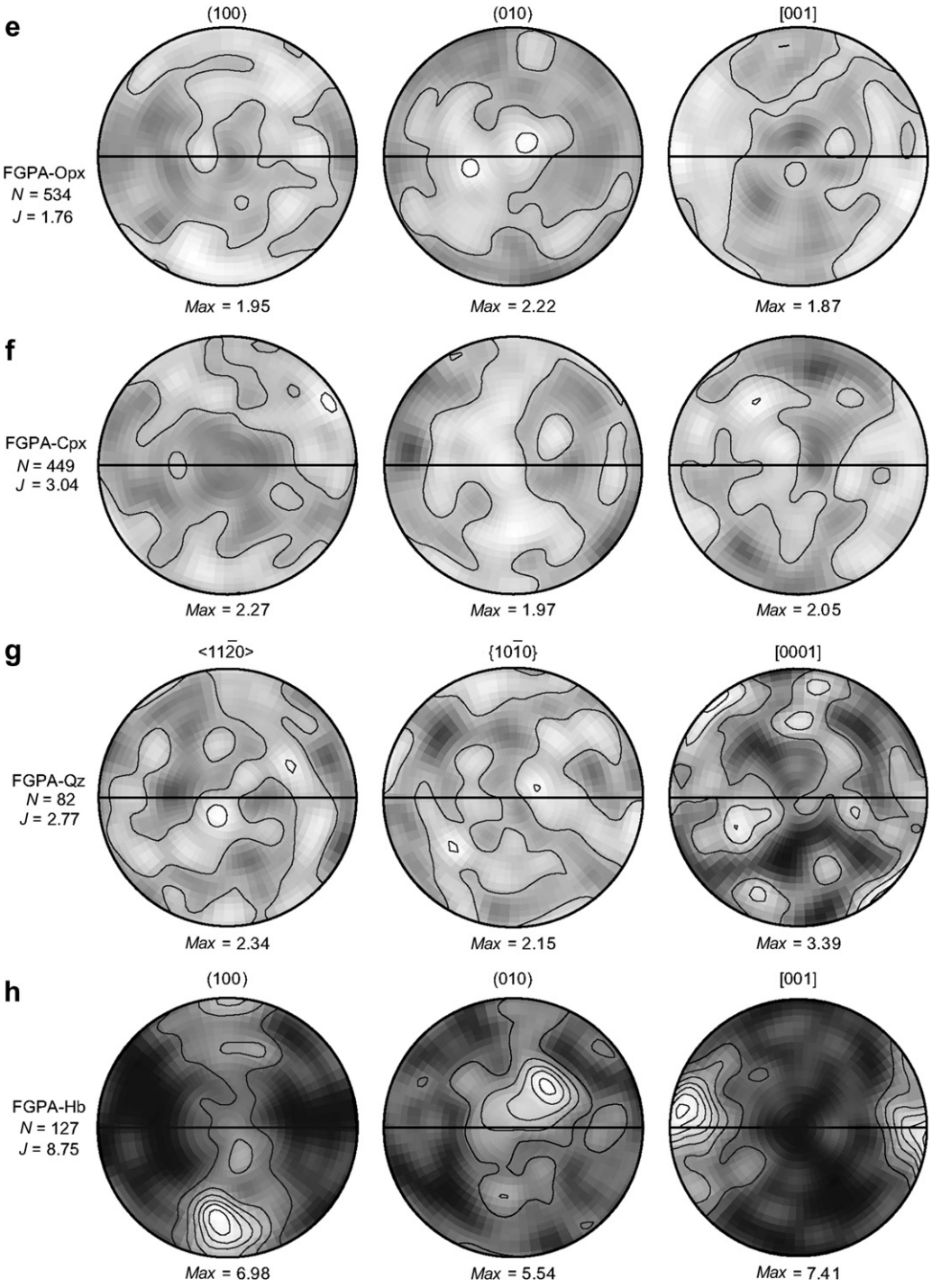

Fig. 6. (*continued*).

Orthopyroxene porphyroclasts are extremely elongate with aspect ratios of up to 20.3, while clinopyroxene porphyroclasts are less elongate with aspect ratios of up to 6.0.

As with monomineralic-aggregate plagioclase in the sample GbM, matrix plagioclase exhibits a moderate ($|\chi^2| \approx 19$) SPO anticlockwise oblique to the foliation trace (Fig. 5c). Matrix pyroxenes and quartz also show weak to moderate ($|\chi^2| = 9$–18) SPOs anticlockwise oblique to the foliation trace (Fig. 5d–f). Matrix hornblende exhibits a distinct ($|\chi^2| \approx 25$) SPO subparallel to the foliation trace (Fig. 5g).

6. Crystallographic orientation data

6.1. Data acquisition and processing

Crystallographic orientations of constituent minerals other than biotite and ilmenite were measured using the SEM-based electron backscatter diffraction (EBSD) technique (e.g. Randle, 2003). EBSD patterns were obtained using an HKL Nordlys EBSD detector mounted on a JEOL JSM-6460 SEM at the Department of Earth Sciences, Chiba University, with an accelerating voltage of 20 kV

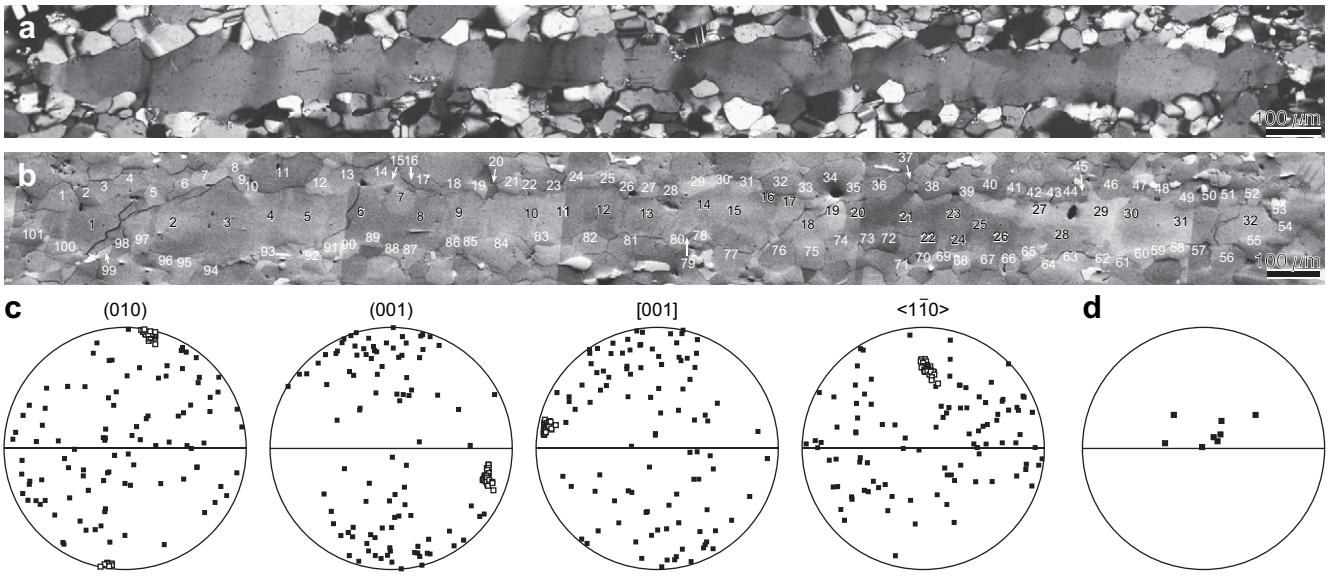

Fig. 7. (a) Optical micrograph (CPL) of the most elongate plagioclase porphyroclast in the sample GbM. (b) Orientation contrast image of the area shown in (a). Black numbers indicate points of crystallographic orientation measurement in the porphyroclast, while white numbers indicate grains in contact with the porphyroclast whose crystallographic orientations are measured. (c) Crystallographic orientations of the plagioclase porphyroclast (open squares) and its adjacent grains (black squares). (d) Misorientation axes of eight pairs of adjacent points (1–2, 3–4, 4–5, 9–10, 10–11, 11–12, 19–20 and 29–30) in the porphyroclast. (c) and (d) are equal-area, lower hemisphere projections with foliation indicated by a horizontal line and lineation direction by its ends.

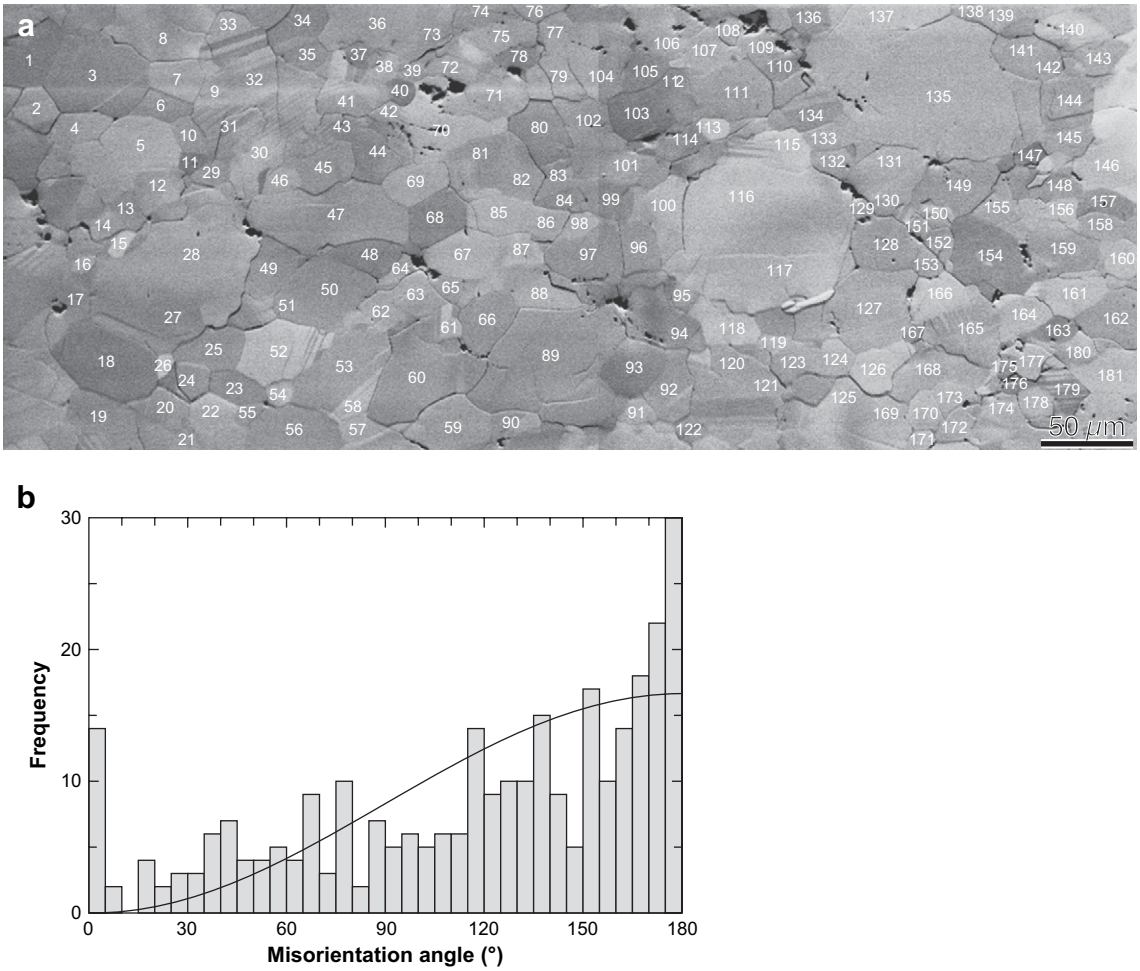

Fig. 8. (a) Orientation contrast image of an area of monomineralic plagioclase aggregate in the sample GbM. White numbers indicate (sub)grains whose crystallographic orientations are measured. (b) Frequency distribution of misorientation angles between pairs of adjacent (sub)grains shown in (a). Solid-line curve indicates a theoretical frequency distribution of misorientation angles between pairs of adjacent (sub)grains in an aggregate of randomly oriented (sub)grains.

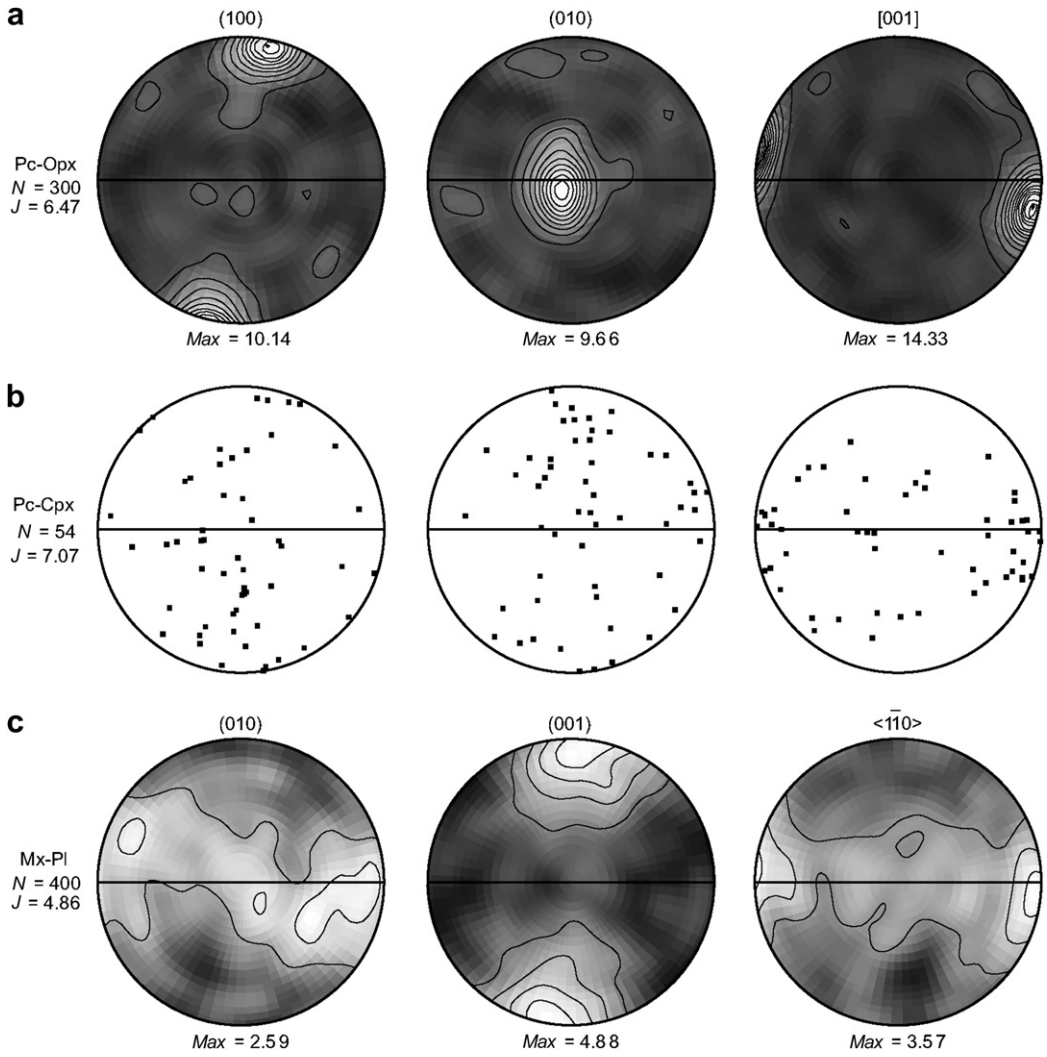

Fig. 9. Crystallographic orientations of constituent mineral grains in the sample GbUM. Equal-area, lower hemisphere projections using David Mainprice's Pf2k. Contoured at multiples of uniform distribution and shaded brighter for higher densities. In each stereogram, foliation is indicated by a horizontal line with lineation direction at its ends. *N*, number of grains measured; *J*, *J*-index value; *Max*, maximum density normalized by uniform distribution. See Table 1 for the abbreviations of minerals and microstructural domains.

and a beam current of 5.2–5.5 nA, and were manually indexed using Channel 5 software (Flamenco) of HKL Technology.

Equal-area, lower hemisphere projections of crystallographic orientation data (Figs. 6, 7c and 9) were prepared using David Mainprice's software (Pf2k). Misorientation axes and angles between adjacent plagioclase (sub)grains (Figs. 7d and 8b) were calculated using Channel 5 software (Manager Data). For each data set of crystallographic-preferred orientation (CPO), the *J*-index value of its orientation distribution function (Bunge, 1982) was calculated using Channel 5 software (Salsa), and was used as a measure of its strength. Although *J*-index values range from 1 for a random orientation to infinity for a single crystal (Bunge, 1982), values calculated from a limited number of data should be interpreted with caution, because they show a tendency to increase with decreasing number of data when other parameters are constant (Wenk, 2002; Skemer et al., 2005).

6.2. Gabbro mylonite sample (GbM)

Porphyroclast orthopyroxene exhibits a strong ($J \approx 6.1$) CPO with (100) and [001] subparallel to the foliation and the lineation, respectively (Fig. 6a). Porphyroclast clinopyroxene shows a CPO similar to, but weaker ($J \approx 5.6$) than the one of porphyroclast orthopyroxene (Fig. 6b).

Porphyroclast plagioclase exhibits a weak CPO with a diffuse girdle of (010) subnormal to the lineation and a diffuse girdle of [001] subparallel to the foliation (Fig. 6c). Although it has a rather high *J*-index value of ≈4.6, this is probably because of the small number of data. An extremely elongate plagioclase porphyroclast (Fig. 7a,b) is oriented such that its (010) and [001] are slightly clockwise oblique to the foliation and the lineation, respectively (open squares in Fig. 7c). Subgrain boundaries whose traces are almost normal to the [001] direction are developed in this porphyroclast (Fig. 7a,c). Misorientation axes between adjacent pairs of subgrains in this porphyroclast are roughly within the foliation plane and perpendicular to the lineation (Fig. 7d). Finer plagioclase grains surrounding and in contact with this porphyroclast, however, have crystallographic orientations mostly unrelated to that of the porphyroclast (black squares in Fig. 7c). Such crystallographic relationships are common in this sample.

Monomineralic-aggregate plagioclase exhibits a clear ($J \approx 5.0$) CPO with (001) and $<1\bar{1}0>$ subparallel, but slightly clockwise oblique to the foliation and the lineation, respectively (Fig. 6d). Misorientation angles between adjacent (sub)grain pairs in a monomineralic plagioclase aggregate (Fig. 8a) exhibit a frequency

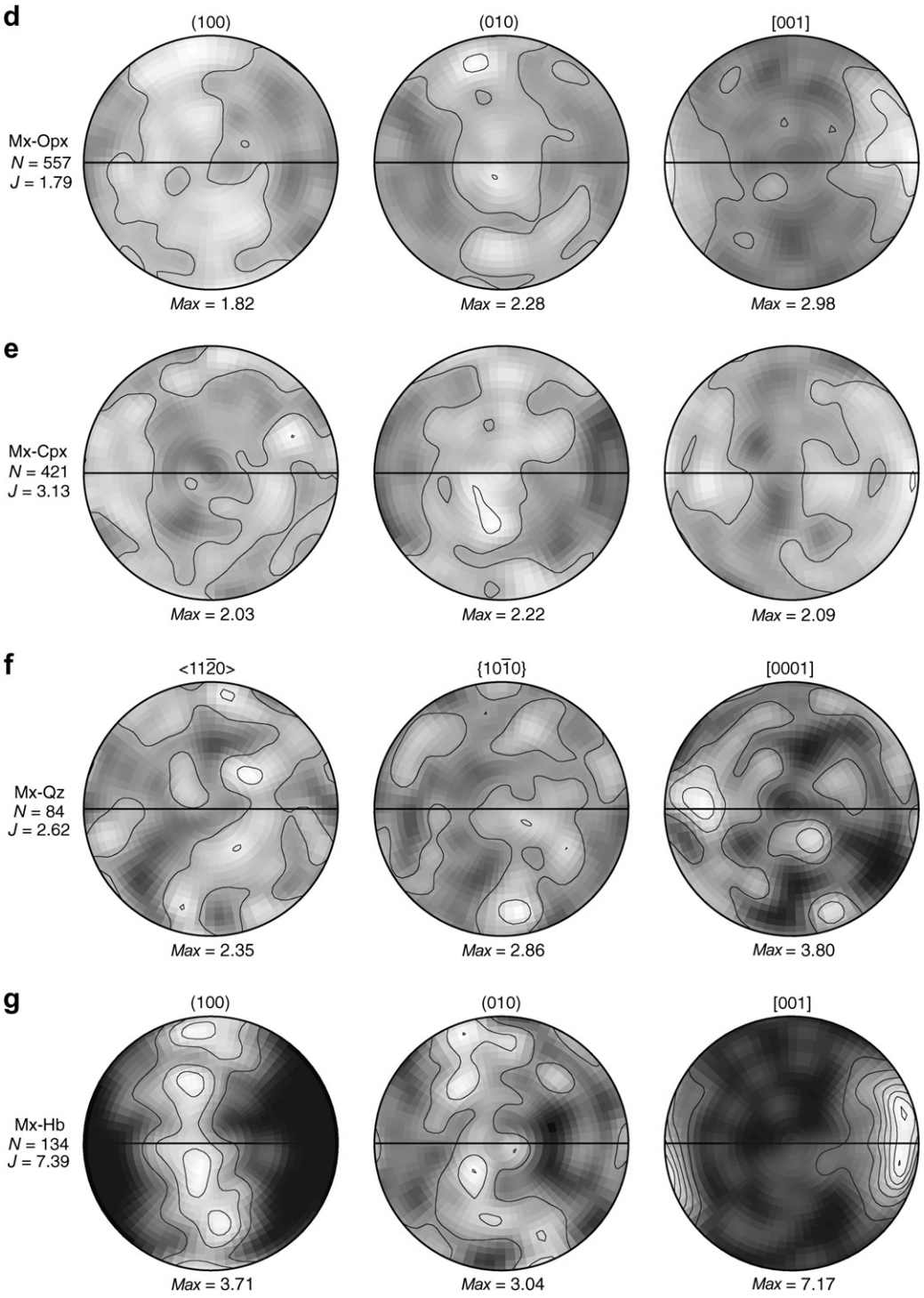

Fig. 9. (*continued*).

distribution with a high frequency at angles smaller than 5°, but with few at angles between 5° and 15° (Fig. 8b). A very high frequency at angles around 180° (Fig. 8b) is attributable to twinning.

In the fine-grained polymineralic aggregate, pyroxenes do not show clear CPOs (Fig. 6e,f), in contrast to porphyroclast pyroxenes. Their (100) planes and [001] axes tend to be preferentially oriented subparallel to the foliation and the lineation, respectively, but their *J*-index values are low: ≈1.8 for orthopyroxene and ≈3.0 for clinopyroxene (Fig. 6e,f). Quartz does not show clear CPO (Fig. 6g). It has a *J*-index value of ≈2.8, which may be overestimated because of the small number of data. In contrast, hornblende exhibits a strong ($J \approx 8.8$) CPO with (100) and [001] subparallel to the foliation and the lineation, respectively (Fig. 6h).

6.3. Gabbro ultramylonite sample (GbM)

Porphyroclast orthopyroxene exhibits a strong ($J \approx 6.5$) CPO with (100) and [001] subparallel and slightly clockwise oblique to the foliation and the lineation, respectively (Fig. 9a). Porphyroclast

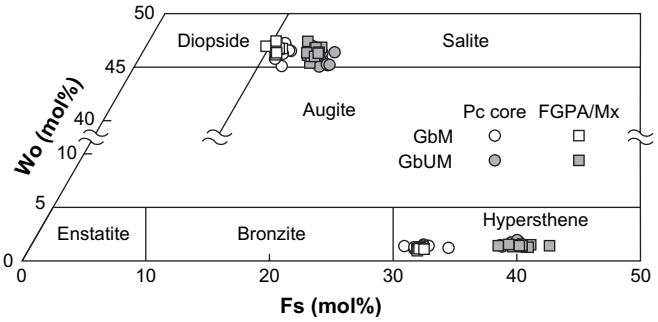

Fig. 10. Chemical compositions of pyroxenes plotted on the ternary diagram of wollastonite ($CaSiO_3$), ferrosilite ($FeSiO_3$), and enstatite ($MgSiO_3$). Classifications of orthopyroxene and clinopyroxene are after Poldervaart (1947), and Poldervaart and Hess (1951), respectively. Wo, wollastonite; Fs, ferrosilite. See Table 1 for the abbreviations of microstructural domains.

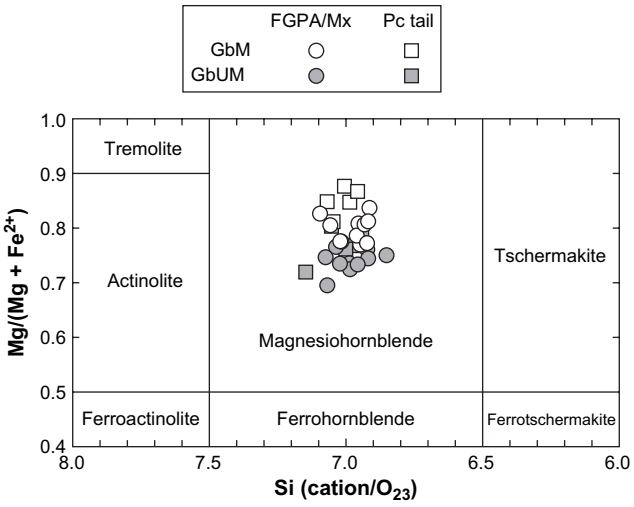

Fig. 12. $Mg/(Mg + Fe^{2+})$ of hornblende plotted against its Si content. Classification of amphiboles is after Leake et al. (1997) for the case of $Ca_B \geq 1.5$, $(Na + K)_A < 0.5$, and $Ca_A < 0.5$. See Table 1 for the abbreviations of microstructural domains.

clinopyroxene may show a similar CPO, but it is unclear because of the limited number of data (Fig. 9b).

Matrix plagioclase exhibits a clear ($J \approx 4.9$) CPO with (001) and $<1\bar{1}0>$ subparallel and slightly clockwise oblique to the foliation and the lineation, respectively (Fig. 9c), similar to the CPO of monomineralic-aggregate plagioclase in the sample GbM. Matrix orthopyroxene shows a weak CPO characterized by a [001] maximum anticlockwise oblique to the lineation and girdles of (100) and (010) around the [001] maximum (Fig. 9d). Although the *J*-index value is as low as ≈1.8, its [001] preferred orientation is distinct as indicated by the maximum density of ≈3 (Fig. 9d). Matrix clinopyroxene exhibits a CPO similar to, but less clear than the one for matrix orthopyroxene (Fig. 9e). Although not clear, there is a tendency for matrix quartz that $\{10\bar{1}0\}$ planes and [0001] axes are preferentially oriented subparallel to the foliation and the lineation, respectively (Fig. 9f). Matrix hornblende exhibits a strong ($J \approx 7.4$) CPO with a [001] maximum subparallel to the lineation and girdles of (100) and (010) around the [001] maximum (Fig. 9g).

7. Chemical compositions of the constituent minerals

Chemical compositions of constituent minerals in three samples (GbM, GbUM and GBGn) were determined by electron microprobe analysis (EPMA) using a JEOL JXA-8900L at the Department of Earth and Planetary Sciences, University of Tokyo. Average chemical compositions are listed in a supplementary table which is available as a PDF file "KSH (JSG) Supplementary Table.pdf" at ftp://ftp-es.s.chiba-u.ac.jp/pub/struct.

Orthopyroxene and clinopyroxene in both samples of GbM and GbUM are hypersthene and salite, respectively (Fig. 10). Their chemical compositions are distinctly different between the two samples; pyroxenes in GbUM are richer in the ferrosilite component compared to those in GbM (Fig. 10). In orthopyroxene porphyroclasts in both samples, Al and Ca contents tend to decrease from their cores to the rims (Fig. 11a). Orthopyroxene grains in the fine-grained polymineralic aggregate or matrix have similar compositions to those in the porphyroclast rims (Fig. 11a). In clinopyroxene porphyroclasts in both samples, there is a tendency from their cores to the rims that Al content decreases, whereas that Ca content increases (Fig. 11b). Clinopyroxene grains in the fine-grained polymineralic aggregate or matrix are poorer in Al content and richer in Ca content compared to those in the porphyroclast rims (Fig. 11b).

The plagioclase in both GbM and GbUM is labradorite. In GbM, porphyroclast plagioclase is An_{53-57}, while monomineralic-aggregate plagioclase is An_{51-55}. No clear difference in composition is

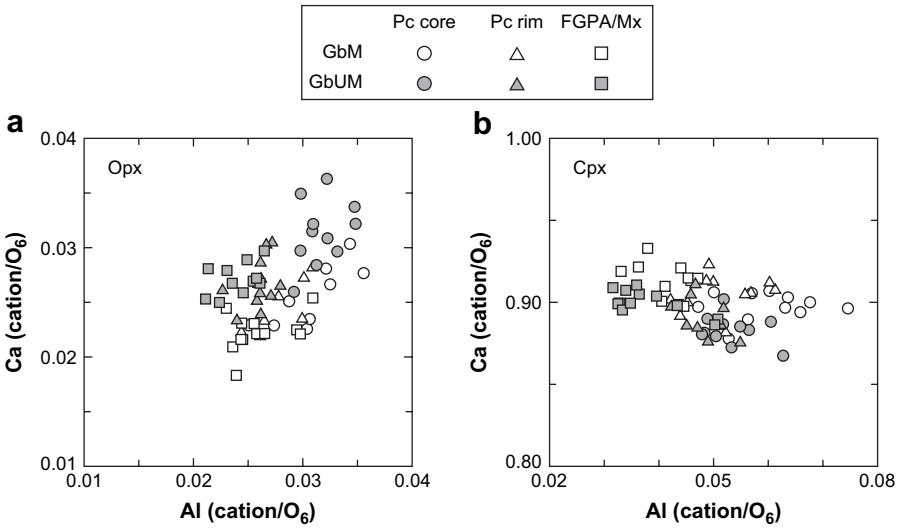

Fig. 11. Ca contents in pyroxenes plotted against their Al contents. See Table 1 for the abbreviations of minerals and microstructural domains.

thus recognized, although plagioclase grains immediately adjacent to hornblende grains in pyroxene porphyroclast tails have unusual compositions of An_{63-75}. In GbUM, matrix plagioclase is An_{49-53}, and slightly poorer in the anorthite component compared to plagioclase in GbM.

Hornblende in both GbM and GbUM is magnesiohornblende (Fig. 12). The chemical compositions of hornblende grains are distinctly different between the two samples as those of pyroxenes. Hornblende grains in GbUM are richer in FeO and poorer in MgO compared to those in GbM; the former have lower $Mg/(Mg + Fe^{2+})$ ratios than the latter (Fig. 12).

8. Discussion

8.1. Mylonitization processes

The matrix of the sample GbM consists of interlayered monomineralic plagioclase aggregates and fine-grained polymineralic aggregates (Fig. 2a). Since these aggregates are not found in the Pankenushi gabbro outside the mylonite zone, they are thought to have formed by mylonitization.

As discussed later, the monomineralic plagioclase aggregate has been formed by dynamic recrystallization, as commonly reported in gabbroic mylonites formed at lower crustal conditions (e.g. Jensen and Starkey, 1985; Olsen and Kohlstedt, 1985; Olesen, 1987; Ji and Mainprice, 1990; Dornbusch et al., 1994; Kruse and Stünitz, 1999; Kruse et al., 2001; Baratoux et al., 2005). The fine-grained polymineralic aggregate composed of orthopyroxene, clinopyroxene, quartz, hornblende, biotite and ilmenite is derived from pyroxene porphyroclast tails (Fig. 2a), and has been formed by mixing of grains derived from the breakdown reaction of two pyroxenes, as discussed below.

The characteristic occurrence of quartz and hornblende around pyroxene porphyroclasts in both samples of GbM and GbUM (Figs. 2c,d and 3c,d) suggests the following breakdown reaction of two pyroxenes:

$$\text{orthopyroxene} + \text{clinopyroxene} + \text{plagioclase} + H_2O = \text{hornblende} + \text{quartz}$$

Unusually high Ca contents (An_{63-75}) found in plagioclase grains adjacent to hornblende grains in pyroxene porphyroclast tails in GbM imply a supply of Na from those plagioclase grains to produce hornblende. The above reaction is known to be a retrograde reaction from granulite facies to amphibolite facies (e.g. Spear, 1993), and is essentially similar to those described by Beach (1980) for some shear-zone rocks in the Lewisian complex of NW Scotland. Because biotite often occurs with hornblende in both GbM and GbUM, it may also be a product of the above reaction.

Quartz commonly occurs as lobate grains along the boundaries of porphyroclasts subparallel to the foliation (Figs. 2c,d and 3c,d), i.e. at sites of high normal stresses during deformation. In contrast, hornblende and biotite commonly occur as euhedral to subhedral grains in porphyroclast tails (Figs. 2c–e and 3c,d), and have therefore grown in low normal stress regions. Such occurrences of quartz, hornblende and biotite around pyroxene porphyroclasts imply a close relationship between the above reaction and deformation, and suggest an incongruent pressure solution process (Beach, 1979). In fact, the Pankenushi gabbro away from the mylonite zone does not show any evidence for the breakdown of either pyroxene. Thus the reaction may have been induced by deformation during mylonitization.

Quartz, hornblende and possibly biotite are thus products of the breakdown reaction of two pyroxenes. Ilmenite is probably derived from the lamellae and/or inclusions in pyroxene porphyroclasts. Pyroxene grains in the fine-grained polymineralic aggregate most likely originate from porphyroclast rims which became isolated during the breakdown of porphyroclasts, as seen in Fig. 2c,d. This explains why fine-grained polymineralic aggregates derived from orthopyroxene porphyroclasts are rich in orthopyroxene (e.g. Fig. 2g) and those derived from clinopyroxene porphyroclasts are rich in clinopyroxene, and also that the chemical compositions of fine-grained pyroxene grains are similar to those of porphyroclast rims, but different to those of porphyroclast cores (Fig. 11).

The mylonitization of the Pankenushi gabbro thus occurred through dynamic recrystallization of plagioclase together with the breakdown reaction of two pyroxenes during retrogression from granulite facies to amphibolite facies. Such mylonitization may be common in lower-crustal gabbroic rocks during their exhumation along faults (cf. Rutter and Brodie, 1992), because they necessarily pass through the granulite–amphibolite facies transition.

The matrix in the sample GbUM is a rather homogeneous mixture, in which grains of constituent minerals in the fine-grained polymineralic aggregate in GbM are scattered throughout the plagioclase aggregate (Fig. 3b). If such a homogeneous mixture in GbUM was formed by mixing of the monomineralic plagioclase and fine-grained polymineralic aggregates seen interlayered in GbM (Fig. 2a), a significant amount of grain boundary sliding would be required. Kenkmann and Dresen (2002) described a similar mylonite–ultramylonite transition in a metagabbro from the Ivrea Zone of NW Italy. They described a microstructural change from compositional layering of monomineralic plagioclase aggregate and amphibole-rich, fine-grained polymineralic aggregate, to a homogeneous mixture of fine-grained amphibole, plagioclase and ilmenite, and ascribed this phase mixing and dispersion also to diffusion-accommodated grain boundary sliding.

GbUM is different from GbM not only in the degree of mylonitization, but also in lithology. GbUM is richer in biotite and ilmenite, and slightly poorer in orthopyroxene than GbM (Table 1). In addition, the chemical compositions of pyroxenes in GbUM are distinctly different from those in GbM; the former are richer in the ferrosilite component (Fig. 10). Such a difference resulted in contrasting chemical compositions of hornblende between the two samples (Fig. 12). The chemical composition of plagioclase in GbUM is also slightly different from that in GbM; the former is slightly poorer in the anorthite component. It may be therefore that such lithological differences reflect different degrees of mylonitization.

8.2. Deformation mechanisms

8.2.1. Porphyroclast pyroxenes

Porphyroclast pyroxenes in both GbM and GbUM show evidence for crystal plastic deformation such as undulose extinction and crystal bending, but none for recovery or dynamic recrystallization. Porphyroclast pyroxenes become more elongate with increasing mylonitization (Figs. 4a,b and 5a,b). In addition, pyroxene grains in the Pankenushi gabbro outside the mylonite zone are less elongate compared to pyroxene porphyroclasts within the mylonite zone. The latter have therefore been elongated by crystal plastic deformation during mylonitization without recovery or dynamic recrystallization, implying that the deformation occurred by glide-controlled dislocation creep. Since the porphyroclasts are likely to be less deformable than the matrix, they must also have undergone rigid rotations within the matrix.

Dornbusch et al. (1994) reported SPOs and CPOs for orthopyroxene in metagabbro mylonites in the Ivrea Zone of NW Italy, which are similar to those of porphyroclast orthopyroxene in GbM and GbUM (Figs. 4a, 5a, 6a and 9a), and attributed them to dislocation glide on (100)[001], which is the most common slip system observed in naturally and experimentally deformed orthopyroxene (e.g. Kohlstedt and Vander Sande, 1973; Ross and Nielsen, 1978). Dornbusch et al. (1994) confirmed by transmission

electron microscopy that (100)[001] is actually the dominant slip system. Porphyroclast orthopyroxene in the Pankenushi gabbro mylonites has likely been deformed by dislocation glide on this slip system.

Porphyroclast clinopyroxene in GbM and GbUM exhibits SPOs and CPOs similar to, but much weaker than those of porphyroclast orthopyroxene (Figs. 4b, 5b, 6b and 9b). (100)[001] is known to be the common slip system also in clinopyroxene (e.g. Avé Lallemant, 1978). Porphyroclast clinopyroxene has therefore likely been deformed by dislocation glide dominantly on (100)[001], similar to, but much less intensely compared to orthopyroxene.

8.2.2. Plagioclase

Plagioclase shows clear evidence for crystal plastic deformation such as undulose extinction, deformation twinning and the development of subgrain boundaries in porphyroclasts (Figs. 2b and 7a), and subgrain boundaries and bulging grain boundaries in aggregate grains (Fig. 2f). Subgrain boundaries developed in some porphyroclasts (e.g. Fig. 7a) provide evidence for dislocation climb and recovery. In addition, similar compositions of porphyroclasts and their surrounding finer-grained, monomineralic-aggregate grains as described above indicate that the latter was formed by an isochemical recrystallization, i.e. dynamic recrystallization in the strict sense (cf. Stünitz, 1988). Crystal plastic deformation accompanied by recovery and dynamic recrystallization implies the deformation of plagioclase by recovery-controlled dislocation creep.

An extremely elongate porphyroclast in GbM (Fig. 7a,b) is oriented suitable for (010)[001] (Fig. 7c), which is known to be the dominant slip system in naturally and experimentally deformed plagioclase (e.g. Olsen and Kohlstedt, 1984; Montardi and Mainprice, 1987; Stünitz et al., 2003). The orientations of subgrain boundaries and their misorientation axes in this porphyroclast (Fig. 7a,d) imply that these subgrain boundaries are tilt boundaries with planar arrays of (010)[001] edge dislocations. Together with the crystallographic orientation, this indicates the dominance of (010)[001] in this porphyroclast. Kruse et al. (2001) also revealed the dominance of this slip system in plagioclase porphyroclasts in an anorthositic gabbro mylonite from the Jotun Nappe of southern Norway.

However, both monomineralic-aggregate grains in GbM and matrix grains in GbUM are preferentially oriented suitable for $(001)<1\bar{1}0>$ in terms of their (001) and $<1\bar{1}0>$ orientations not only subparallel to, but also clockwise oblique to the foliation and the lineation, respectively (Figs. 6d and 9c), suggesting the dominance of this slip system in dynamically recrystallized grains. Although $(001)1/2<1\bar{1}0>$ is thought to be secondary to (010)[001] in plagioclase (Olsen and Kohlstedt, 1984; Kruse and Stünitz, 1999; Kruse et al., 2001; Stünitz et al., 2003), its dominance has not been reported so far. This implies that the dominant slip system operating in the recrystallized grains was different from that in the porphyroclasts, and that dynamic recrystallization was not host-grain controlled, as discussed below.

Dynamically recrystallized grains surrounding and in contact with porphyroclasts have crystallographic orientations mostly unrelated to those of porphyroclasts (Fig. 7c), and are preferentially oriented suitable for $(001)1/2<1\bar{1}0>$ as are many other recrystallized grains (Figs. 6d and 7c). There are few subgrain boundaries with misorientation angles between 5° and 15° in dynamically recrystallized grains (Fig. 8b), and this gap cannot be explained by subgrain rotation during dynamic recrystallization (cf. Trimby et al., 2000). These lines of evidence indicate that dynamic recrystallization of plagioclase occurred by grain boundary migration, but not by subgrain rotation, despite the recognition of subgrain boundaries in some porphyroclasts (Fig. 7a). Porphyroclasts unfavorably oriented for the $(001)1/2<1\bar{1}0>$ slip were therefore being consumed by their surrounding recrystallized grains (Fig. 2b). The presence of bulging grain boundaries in recrystallized grains (Fig. 2f) suggests that bulging recrystallization (Stipp et al., 2002a,b; Tullis, 2002) was dominant.

8.2.3. Pyroxenes and quartz in fine-grained polymineralic aggregate or matrix

Fine-grained polymineralic-aggregate pyroxenes in GbM do not show SPOs nor CPOs (Figs. 4e,f, and 6e,f). If fine-grained polymineralic-aggregate pyroxene grains in GbM originate from porphyroclast rims as discussed in Section 8.1, they should have initially had CPOs as strong as those of pyroxene porphyroclasts. Although their CPOs are similar in pattern to those of the pyroxene porphyroclasts, they are significantly weaker. Together with fine grain sizes (average <20 μm; Table 1) and small aspect ratios ($\bar{R} < 1.3$; Fig. 4e,f), these features strongly suggest that the deformation of these pyroxene grains occurred dominantly by grain boundary sliding.

Quartz in the fine-grained polymineralic aggregate in GbM also exhibits very weak SPO and CPO (Figs. 4g and 6g). It also has fine grain sizes (average ≈8 μm; Table 1) and small aspect ratios ($\bar{R} \approx 1.3$; Fig. 4g). Quartz grains have therefore also likely been deformed dominantly by grain boundary sliding.

As discussed in Section 8.1, the fine-grained polymineralic aggregate in GbM is formed by mixing of mineral grains derived from the breakdown reaction of pyroxenes. This mixing of mineral grains was likely facilitated by the grain boundary sliding of pyroxene and quartz grains. The reaction necessarily accompanies grain boundary diffusion, which must have accommodated their deformation by grain boundary sliding.

The SPOs of matrix pyroxene and quartz grains in GbUM are, however, stronger than those of fine-grained polymineralic-aggregate pyroxene and quartz grains in GbM (Figs. 4e–g and 5d–f). Although the CPOs of these mineral grains are not noticeably different in strength between the two samples, their patterns are more clearly defined in GbUM (Figs. 6e–g and 9d–f). These features suggest crystal plastic deformation of pyroxenes and quartz in the GbUM matrix. In contrast to those in the fine-grained polymineralic aggregate in GbM, pyroxene and quartz grains in GbUM matrix are rather isolated within the plagioclase aggregates (Fig. 3a,b). Pyroxene grains would have then behaved as pyroxene porphyroclasts, and quartz grains would have been more deformed than plagioclase. The CPO of quartz grains (Fig. 9f) suggests the activation of $\{10\bar{1}0\}[0001]$ slip, which is known as dominant in quartz at high temperatures (e.g. Mainprice et al., 1986). In addition to crystal plastic deformation, isolated pyroxene grains in GbUM matrix may also have undergone rigid rotations, as suggested by girdle distributions of orthopyroxene (100) and (010) (Fig. 9d).

8.2.4. Hornblende

Hornblende grains in both GbM and GbUM exhibit an SPO subparallel to the foliation trace as well as a strong CPO with (100) and [001] subparallel to the foliation and the lineation, respectively (Figs. 4h, 5g, 6h and 9g). (100)[001] is known as the dominant slip system in experimentally and naturally deformed hornblende (e.g. Morrison-Smith, 1976; Skrotzki, 1990). Although hornblende grains are preferentially oriented suitably for this slip system, it is unlikely that they are crystal-plastically deformed, because they are commonly euhedral to subhedral (e.g. Fig. 2e) showing no evidence for crystal plastic deformation. Euhedral to subhedral shapes of hornblende grains are attributable to their growth in pyroxene porphyroclast tails during the breakdown reaction of pyroxenes. Imon et al. (2004) demonstrated that preferred growth of hornblende in a stress field (e.g. Schwerdtner, 1964; Hara et al., 1983) resulted in a CPO with (100) and [001] subparallel to the foliation and the lineation, respectively, in amphibolites from the Ryoke metamorphic belt of SW Japan. Hornblende is known to behave

passively both in nature and in experiments unless it forms a stress-supporting framework (e.g. Rutter and Brodie, 1992). It is therefore likely that hornblende grains behaved passively after their growth in pyroxene porphyroclast tails, and that they retained the SPO and CPO formed during their growth.

The SPO of hornblende grains in GbUM is stronger than that in GbM (Figs. 4h and 5g). In addition, (100) and (010) planes of hornblende grains in GbUM are distributed along a girdle around the lineation (Fig. 9g). These changes in SPO and CPO of hornblende grains with increasing mylonitization may be attributed to rigid rotations of grains relative to the matrix.

8.3. Rheology

The modal abundance of two pyroxenes (more than 80% in total; Table 1) means that they are likely to have formed a stress-supporting framework in the fine-grained polymineralic aggregates in GbM (e.g. Fig. 2g). The two pyroxenes, deformed dominantly by grain boundary sliding, have therefore likely controlled the rheology of the fine-grained polymineralic aggregates during the mylonitization. The occurrence of the fine-grained polymineralic aggregates extending from pyroxene porphyroclasts tails (Fig. 2a) implies that strain was localized into those aggregates, and that they were weaker than the monomineralic plagioclase aggregate deformed by dislocation creep. The localization of strain into reaction-derived, fine-grained polymineralic aggregates is now well documented in nature as well as in experiments (e.g. Furusho and Kanagawa, 1999; Newman et al., 1999; Stünitz and Tullis, 2001; Handy and Stünitz, 2002; Tsurumi et al., 2003; de Ronde et al., 2004, 2005).

Although the fine-grained polymineralic aggregates are interlayered with the monomineralic plagioclase aggregates in GbM, the former seems to be too limited in amount (≈23%; Table 1) to form continuous layers (Fig. 2a) and hence to control the rock rheology. In contrast, the modal abundance (≈64%; Table 1) and continuous layers of the monomineralic plagioclase aggregate (Fig. 2a) suggest that the latter, deformed by dislocation creep, has controlled the rock rheology of GbM. The modal abundance of plagioclase aggregates (≈65%; Table 1) as well as their development as a stress-supporting framework in the GbUM matrix (e.g. Fig. 3b) indicates that aggregate plagioclase, deformed by dislocation creep, has also controlled the rock rheology of GbUM. Thus the strength of gabbro during its mylonitic deformation at lower crustal conditions is likely approximated by the dislocation creep strength of plagioclase, as previously suggested (e.g. Rutter and Brodie, 1992; Dornbusch et al., 1994).

8.4. Pressure–temperature estimates

The mineral chemistry data of the Pankenushi gabbro and its adjacent felsic gneiss used for geothermobarometry applications below are listed in a supplementary table available at ftp://ftp-es.s.chiba-u.ac.jp/pub/struct.

Applying Hoisch's (1990) garnet–biotite–plagioclase barometry, and Hodges and Spear's (1982) garnet–biotite thermometry to the average chemical compositions of garnet, biotite and plagioclase grains in the sample GBGn adjacent to the mylonite zone (Fig. 1b), we estimated its metamorphic pressure and temperature to be ≈600 MPa and ≈740 °C (Table 2). Because the Pankenushi gabbro is considered to have been intruded during a metamorphic peak in the Hidaka metamorphic Main Zone (Komatsu et al., 1994), the metamorphic pressure recorded in GBGn likely indicates a depth at which the Pankenushi gabbro was intruded.

A number of thermometric techniques were then applied, including the two-pyroxene method (Kretz, 1982), the hornblende–plagioclase method (Blundy and Holland, 1990) which was used for hornblende in pyroxene porphyroclast tails and its adjacent plagioclase, and the hornblende method (Schumacher et al., 1990) using Ti contents for hornblende coexisting with ilmenite. Porphyroclast pyroxenes record a temperature of ≈800 °C, whereas matrix pyroxenes, hornblende and its adjacent plagioclase record temperatures of 660–700 °C (Table 2). The temperatures of ≈800 °C, which are higher than the metamorphic temperature of ≈740 °C, likely indicate a temperature of the Pankenushi gabbro during its intrusion at a pressure of ≈600 MPa, while the temperatures of 660–700 °C indicate a temperature range during the decomposition reaction of pyroxenes and hence its mylonitization.

Table 2
Pressure–temperature conditions estimated for the three samples

Sample	Microstructural domain	Geothermobarometry				
		1	2	3	4	5
GBGn		≈600 MPa	≈740 °C			
GbM	Pc core			783 °C		
	Pc tail				663 °C	≈660 °C
	FGPA			716 °C		≈675 °C
GbUM	Pc core			795 °C		
	Pc tail				704 °C	≈665 °C
	Mx			695 °C		≈670 °C

1, garnet–biotite–plagioclase barometry of Hoisch (1990); 2, garnet–biotite thermometry of Hodges and Spear (1982); 3, two-pyroxene thermometry of Kretz (1982); 4, hornblende–plagioclase thermometry of Blundy and Holland (1990); 5, hornblende thermometry of Schumacher et al. (1990). See Table 1 for the abbreviations of microstructural domains.

9. Conclusions

1. The mylonitization of the Pankenushi gabbro in the Hidaka metamorphic belt of central Hokkaido, Japan, occurred through dynamic recrystallization of plagioclase and a retrograde reaction from granulite facies to amphibolite facies (orthopyroxene + clinopyroxene + plagioclase + H_2O = hornblende + quartz).
2. The dynamic recrystallization of plagioclase produced a monomineralic plagioclase aggregate, while the reaction produced a fine-grained (≤100 μm) polymineralic aggregate composed of orthopyroxene, clinopyroxene, quartz, hornblende, biotite and ilmenite. The monomineralic plagioclase and fine-grained polymineralic aggregates are interlayered to define the mylonitic foliation, while the latter is mixed with the former by grain boundary sliding to form a rather homogeneous polymineralic matrix in an ultramylonite.
3. Plagioclase has been deformed by recovery-controlled dislocation creep. Dynamic recrystallization of plagioclase occurred by grain boundary migration. Although (010)[001] is found to have been dominant in an extremely elongate porphyroclast, $(001)1/2<1\bar{1}0>$ was likely the dominant slip system in dynamically recrystallized grains in the matrix.
4. Porphyroclast pyroxenes have been deformed by dislocation glide on (100)[001] as well as by rigid rotation in the matrix. Clinopyroxene porphyroclasts are much less deformed than orthopyroxene porphyroclasts.
5. Pyroxene and quartz grains in the fine-grained polymineralic aggregates of the mylonite have been deformed dominantly by diffusion-accommodated grain boundary sliding, while these grains are scattered and isolated in plagioclase aggregate in the ultramylonite matrix where they have begun to undergo crystal plastic deformation as well as rigid rotation of pyroxene grains.
6. Euhedral to subhedral hornblende grains have grown in pyroxene porphyroclast tails during the breakdown reaction of the two pyroxenes, and they have then behaved passively in

the fine-grained polymineralic aggregate or matrix during subsequent mylonitic deformation.

7. Pyroxene grains deformed by diffusion-accommodated grain boundary sliding controlled the rheology of the fine-grained polymineralic aggregates. Although strain is localized into the fine-grained polymineralic aggregates, they were too limited in volume to control the bulk rock rheology, which was controlled by plagioclase aggregates deformed by dislocation creep. Thus the strength of gabbro during its mylonitic deformation at lower crustal conditions likely corresponds to the dislocation creep strength of plagioclase.
8. The geothermobarometry applications to chemical compositions of constituent minerals in the Pankenushi gabbro and its adjacent felsic gneiss suggest that the gabbro was intruded at ≈600 MPa and ≈800 °C, and was mylonitized under a temperature range of 660–700 °C.

Acknowledgments

We thank M. Ono for her logistic support during H.S.'s field work, H. Yoshida for assisting with EPMA analyses, D. Mainprice for his advice during the initial setup of an EBSD system at Chiba University as well as providing reflector databases of plagioclase with different compositions, T. Okudaira for providing his program on Blundy and Holland's (1990) thermometry, Y. Suda for providing his program on Kretz's (1982) thermometry, and S. Yoshida for improving the English text. We also thank K. Brodie, G. Dresen and J. Kruhl for their helpful reviews, and R. Holdsworth for his editorial work. This study was supported by JSPS grants to K.K. (#13304042 and #17340159) and to Y.H. (#14340158).

References

Arita, K., Shingu, H., Itaya, T., 1993. K–Ar geochronological constraints on tectonics and exhumation of the Hidaka metamorphic belt, Hokkaido, northern Japan. Journal of Mineralogy, Petrology and Economic Geology 88, 101–113.

Avé Lallemant, H.G., 1978. Experimental deformation of diopside and websterite. Tectonophysics 48, 1–27.

Baratoux, L., Schulmann, K., Ulrich, S., Lexa, O., 2005. Contrasting microstructures and deformation mechanisms in metagabbro mylonites contemporaneously deformed under different temperatures (c. 650°C and 750°C). In: Gapais, D., Brun, J.P., Cobbold, P.R. (Eds.), Deformation Mechanisms, Rheology and Tectonics: from Minerals to the Lithosphere. Special Publications 243. Geological Society, London, pp. 97–125.

Beach, A., 1979. Pressure solution as a metamorphic process in deformed terrigenous sedimentary rocks. Lithos 12, 51–58.

Beach, A., 1980. Retrogressive metamorphic processes in shear zones with special reference to the Lewisian complex. Journal of Structural Geology 2, 257–263.

Blundy, J.D., Holland, T.J.B., 1990. Calcic amphibole equilibria and a new amphibole-plagioclase geothermometer. Contributions to Mineralogy and Petrology 104, 208–224.

Brodie, K.H., 1995. The development of oriented symplectites during deformation. Journal of Metamorphic Geology 13, 499–508.

Bunge, H.-J., 1982. Texture Analysis in Materials Science—Mathematical Methods. Butterworths, London.

de Ronde, A.A., Heilbronner, R., Stünitz, H., Tullis, J., 2004. Spatial correlation of deformation and mineral reaction in experimentally deformed plagioclase–olivine aggregates. Tectonophysics 389, 93–109.

de Ronde, A.A., Stünitz, H., Tullis, J., Heilbronner, R., 2005. Reaction-induced weakening of plagioclase–olivine composites. Tectonophysics 409, 85–106.

Dornbusch, H.-J., Weber, K., Skrotzki, W., 1994. Development of microstructure and texture in high-temperature mylonites from the Ivrea Zone. In: Bunge, H.J., Siegesmund, S., Skrotzki, W., Weber, K. (Eds.), Textures of Geological Materials. DGM Informationsgesellschaft, Oberursel, pp. 187–201.

Furusho, M., Kanagawa, K., 1999. Transformation-induced strain localization in a lherzolite mylonite from the Hidaka metamorphic belt of central Hokkaido, Japan. Tectonophysics 313, 411–432.

Handy, M.R., Stünitz, H., 2002. Strain localization by fracturing and reaction weakening—a mechanism for initiating exhumation of subcontinental mantle beneath rifted margins. In: de Meer, S., Drury, M.R., de Bresser, J.H.P., Pennock, G.M. (Eds.), Deformation Mechanisms, Rheology and Tectonics: Current Status and Future Perspectives. Special Publications 200. Geological Society, London, pp. 387–407.

Hara, I., Shiota, T., Maeda, M., Miyaoka, H., 1983. Deformation and recrystallization of amphiboles in Sambagawa schist, with special reference to history of Sambagawa metamorphism. Journal of Science, Hiroshima University, Series C 8, 135–148.

Hodges, K.V., Spear, F.S., 1982. Geothermometry, geobarometry and the Al_2SiO_5 triple point at Mt. Moosilauke, New Hampshire. American Mineralogist 67, 1118–1134.

Hoisch, T.D., 1990. Empirical calibration of six geobarometers for the mineral assemblage quartz + muscovite + biotite + plagioclase + garnet. Contributions to Mineralogy and Petrology 104, 225–234.

Imon, R., Okudaira, T., Kanagawa, K., 2004. Development of shape- and lattice-preferred orientations of amphibole grains during initial cataclastic deformation and subsequent deformation by dissolution–precipitation creep in amphibolites from the Ryoke metamorphic belt, SW Japan. Journal of Structural Geology 26, 793–805.

Jensen, L.N., Starkey, J., 1985. Plagioclase microfabrics in a ductile shear zone from the Jotun Nappe, Norway. Journal of Structural Geology 7, 527–539.

Ji, S., Mainprice, D., 1990. Recrystallization and fabric development in plagioclase. Journal of Geology 98, 65–79.

Kenkmann, T., 2000. Processes controlling the shrinkage of porphyroclasts in gabbroic shear zones. Journal of Structural Geology 22, 471–487.

Kenkmann, T., Dresen, G., 2002. Dislocation microstructure and phase distribution in a lower crustal shear zone—an example from the Ivrea-Zone, Italy. International Journal of Earth Sciences 91, 445–458.

Kimura, G., 1986. Collision orogeny at arc–arc junctions in the Japanese Islands. The Island Arc 5, 262–275.

Kiyokawa, S., 1992. Geology of the Idonnappu Belt, central Hokkaido, Japan: Evolution of a Cretaceous accretionary complex. Tectonics 11, 1180–1206.

Kohlstedt, D.L., Vander Sande, J.B., 1973. Transmission electron microscopy investigation of the defect microstructure of four natural orthopyroxenes. Contributions to Mineralogy and Petrology 42, 169–180.

Komatsu, M., Miyashita, S., Maeda, J., Osanai, Y., Toyoshima, T., 1983. Disclosing of a deepest section of continental-type crust up-thrust as the final event of collision of arcs in Hokkaido, North Japan. In: Hashimoto, M., Uyeda, S. (Eds.), Accretion Tectonics in the Circum-Pacific Regions. TERRAPUB, Tokyo, pp. 149–165.

Komatsu, M., Toyoshima, T., Osanai, Y., Arai, M., 1994. Prograde and anatectic reactions in the deep arc crust exposed in the Hidaka metamorphic belt, Hokkaido, Japan. Lithos 33, 31–49.

Kretz, R., 1982. Transfer and exchange equilibria in a portion of the pyroxene quadrilateral as deduced from natural and experimental data. Geochimica et Cosmochimica Acta 46, 411–421.

Kruse, R., Stünitz, H., 1999. Deformation mechanisms and phase distribution in mafic high-temperature mylonites from the Jotun Nappe, southern Norway. Tectonophysics 303, 223–249.

Kruse, R., Stünitz, H., Kunze, K., 2001. Dynamic recrystallization processes in plagioclase porphyroclasts. Journal of Structural Geology 23, 1781–1802.

Leake, B.E., Woolley, A.R., Arps, C.E.S., Birch, W.D., Gilbert, M.C., Grice, J.D., Hawthorne, F.C., Kato, A., Kisch, H.J., Krivovichev, V.G., Linthout, K., Laird, J., Mandarino, J.A., Maresch, W.V., Nickel, E.H., Rock, N.M.S., Schumacher, J.C., Smith, D.C., Stephenson, N.C.N., Ungaretti, L., Whittaker, E.J.W., Youzhi, G., 1997. Nomenclature of amphiboles: Report of the subcommittee on amphiboles of the international mineralogical association, commission on new minerals and mineral names. The Canadian Mineralogist 35, 219–246.

Maeda, J., Kagami, H., 1996. Interaction of a spreading ridge and accretionary prism: Implications from MORB magmatism in the Hidaka magmatic zone, Hokkaido, Japan. Geology 24, 31–34.

Mainprice, D., Bouchez, J.-L., Blumenfeld, P., Tubià, J.M., 1986. Dominant *c* slip in naturally deformed quartz: Implications for dramatic plastic softening at high temperature. Geology 14, 819–822.

Miyashita, S., 1983. Reconstruction of the ophiolite succession in the western zone of the Hidaka Metamorphic Belt, Hokkaido. Journal of the Geological Society of Japan 89, 69–86.

Montardi, Y., Mainprice, D., 1987. A transmission electron microscopic study of the natural plastic deformation of calcic plagioclase (An 68–70). Bulletin de Minéralogie 110, 1–14.

Morrison-Smith, D.J., 1976. Transmission electron microscopy of experimentally deformed hornblende. American Mineralogist 61, 272–280.

Newman, J., Lamb, W.M., Drury, M.R., Vissers, R.L.M., 1999. Deformation processes in a peridotite shear zone: Reaction-softening by an H_2O-deficient, continuous net transfer reaction. Tectonophysics 303, 193–222.

Olesen, N.Ø., 1987. Plagioclase fabric development in a high-grade shear zone, Jotunheimen, Norway. Tectonophysics 142, 291–308.

Olsen, T.S., Kohlstedt, D.L., 1984. Analysis of dislocations in some naturally deformed plagioclase feldspars. Physics and Chemistry of Minerals 11, 153–160.

Olsen, T.S., Kohlstedt, D.L., 1985. Natural deformation and recrystallization of some intermediate plagioclase feldspars. Tectonophysics 111, 107–131.

Osanai, Y., Komatsu, M., Owada, M., 1991. Metamorphism and granite genesis in the Hidaaka Metamorphic Belt, Hokkaido, Japan. Journal of Metamorphic Geology 9, 111–124.

Owada, M., Osanai, Y., Kagami, H., 1991. Timing of anatexis in the Hidaka metamorphic belt, Hokkaido, Japan. Journal of the Geological Society of Japan 97, 751–754.

Poldervaart, A., 1947. The relationship of orthopyroxene to pigeonite. Mineralogical Magazine 28, 164–172.

Poldervaart, A., Hess, H.H., 1951. Pyroxenes in the crystallization of basaltic magmas. Journal of Geology 59, 472–489.

Prior, D.J., Trimby, P.W., Weber, U.D., Dingley, D.J., 1996. Orientation contrast imaging of microstructures in rocks using forescatter detectors in the scanning electron microscope. Mineralogical Magazine 60, 859–869.

Randle, V., 2003. Microtexture Determination and Its Applications, second ed. Maney, London.

Ross, J.V., Nielsen, K.C., 1978. High-temperature flow of wet polycrystalline enstatite. Tectonophysics 44, 233–261.

Rutter, E.H., Brodie, K.H., 1992. Rheology of the lower crust. In: Fountain, D.M., Arculus, R., Kay, R.W. (Eds.), Continental Lower Crust. Elsevier, Amsterdam, pp. 201–267.

Schumacher, J.C., Hollocher, K.T., Robinson, P., Tracy, R.J., 1990. Progressive reactions and melting in the Acadian metamorphic high of central Massachusetts and southwestern New Hampshire, USA. In: Ashworth, J.R., Brown, M. (Eds.), High Temperature Metamorphism and Crustal Anatexis. Unwin Hyman, London, pp. 198–234.

Schwerdtner, W.M., 1964. Preferred orientation of hornblende in a banded hornblende gneiss. American Journal of Science 262, 1212–1229.

Skemer, P., Katayama, I., Jiang, Z., Karato, S., 2005. The misorientation index: Development of a new method for calculating the strength of lattice-preferred orientation. Tectonophysics 411, 157–167.

Skrotzki, W., 1990. Microstructure of hornblende of a mylonitic amphibolite. In: Knipe, R.J., Rutter, E.H. (Eds.), Deformation Mechanisms, Rheology and Tectonics. Special Publications 54. Geological Society, London, pp. 321–325.

Spear, F.S., 1993. Metamorphic Phase Equilibria and Pressure–Temperature-Time Paths. Mineralogical Society of America, Washington, DC.

Stipp, M., Stünitz, H., Heilbronner, R., Schmid, S.M., 2002a. Dynamic recrystallization of quartz: correlation between natural and experimental conditions. In: de Meer, S., Drury, M.R., de Bresser, J.H.P., Pennock, G.M. (Eds.), Deformation Mechanisms, Rheology and Tectonics: Current Status and Future Perspectives. Special Publications 200. Geological Society, London, pp. 171–190.

Stipp, M., Stünitz, H., Heilbronner, R., Schmid, S.M., 2002b. The eastern Tonale fault zone: a 'natural laboratory' for crystal plastic deformation of quartz over a temperature range from 250 to 700°C. Journal of Structural Geology 24, 1861–1884.

Stünitz, H., 1998. Syndeformational recrystallization—dynamic or compositionally induced? Contributions to Mineralogy and Petrology 131, 219–236.

Stünitz, H., Tullis, J., 2001. Weakening and strain localization produced by syndeformational reaction of plagioclase. International Journal of Earth Sciences 90, 136–148.

Stünitz, H., Fitz Gerald, J.D., Tullis, J., 2003. Dislocation generation, slip systems, and dynamic recrystallization in experimentally deformed plagioclase single crystals. Tectonophysics 372, 215–233.

Toyoshima, T., 1998. Gabbro mylonite developed along a crustal-scale décollement. In: Snoke, A.W., Tullis, J., Todd, V.R. (Eds.), Fault-related Rocks—A Photographic Atlas. Princeton University Press, Princeton, pp. 426–427.

Toyoshima, T., Komatsu, M., Shimura, T., 1994. Tectonic evolution of lower crustal rocks in an exposed magmatic arc section in the Hidaka Metamorphic Belt, Hokkaido, northern Japan. The Island Arc 3, 182–198.

Trimby, P.W., Drury, M.R., Spiers, C.J., 2000. Recognising the crystallographic signature of recrystallization processes in deformed rocks: a study of experimentally deformed rocksalt. Journal of Structural Geology 22, 1609–1620.

Tsurumi, J., Hosonuma, H., Kanagawa, K., 2003. Strain localization due to a positive feedback of deformation and myrmekite-forming reaction in granite and aplite mylonites along the Hatagawa Shear Zone of NE Japan. Journal of Structural Geology 25, 557–584.

Tullis, J., 2002. Deformation of granitic rocks: experimental studies and natural examples. In: Karato, S., Wenk,., H.-R. (Eds.), Plastic Deformation of Minerals and Rocks. Reviews in Mineralogy and Geochemistry, 51, pp. 51–95.

Ueda, H., Kawamura, M., Iwata, K., 1993. Occurrence of the Paleocene radiolarian fossils from the Idon'nappu Belt, central part of Hokkaido, Northern Japan. Journal of the Geological Society of Japan 99, 565–568.

Wenk, H.-R., 2002. Texture and anisotropy. In: Karato, S., Wenk, H.-R. (Eds.), Plastic Deformation of Minerals and Rocks. Reviews in Mineralogy and Geochemistry, 51, pp. 291–329.

Wheeler, J., 1984. A new plot to display the strain of elliptical markers. Journal of Structural Geology 6, 417–423.